2018

Correction of the fringe order errors for fringe projection profilometry

Naixin Li
University of Wollongong

Correction of the fringe order errors for fringe projection profilometry

NAIXIN LI

Supervisors:

Professor Jiangtao Xi

Associate Professor Yanguang Yu

Dr. Jun Tong

This thesis is presented as part of the requirement for the conferral of the degree:

Master of Philosophy

The University of Wollongong

School of Electrical, Computer, Telecommunications Engineering

Faculty of Engineering and Information Sciences

<< March>> <<2018>>

Dedicated to My Family and Research

ACKNOWLEDGEMENT

First and foremost, I would like to extend my gratefulness to my supervisor, Professor Jiangtao XI, who has guided, encouraged and been patient to me throughout the entire research to help me understand the procedure of academic research.

I am considerably grateful to my co-supervisor, Associate Professor Yanguang YU and Dr. Jun TONG who inspired me and gave advises for my entire research.

Additionally, this thesis would not have been possible without the technical support and the help of the fellow of the Optoelectronic Signal Processing Research (OSPR) laboratory, and staffs of the School of Electrical, Computer and Telecommunications Engineering.

Eventually, I would like to thank my family. Thanks to their support on my study and life in Australia, I have an opportunity to finish my research and thesis.

Naixin LI
2018

THESIS CERTIFICATION

CERTIFICATION

I, Naixin LI, declare that this thesis submitted in fulfilment of the requirements for the conferral of the degree Master of Philosophy, from the University of Wollongong, is wholly my own work unless otherwise referenced or acknowledged. This document has not been submitted for qualifications at any other academic institution.

_____

Naixin LI

23rd March 2018

LIST OF ABBREVIATIONS

3D	three-Dimension or three-Dimensional
FPP	fringe projection profilometry
FTP	Fourier transform profilometry
PSP	phase-shifting profilometry
PMP	phase-measuring profilometry
MP	Moire technique
FOE	fringe order error
QGPU	quality-guided phase unwrapping
MMP	modulation measurement profilometry
TOF	time-of-flight

CONTENTS

LIST OF FIGURES AND TABLES

ABSTRACT

Non-contact three-dimensional (abbreviated as 3D) Fringe projection profilometry (abbreviated as FPP) counts as a method of reconstructing the shape of object surface. This technique has been extensively used in many areas, e.g. computer vision, biomedical research, industrial applications, and virtual reality. Using a FPP, sinusoidal patterns are projected on the object surface by mean of a digital projector, and subsequently a camera captures the reflected patterns deformed by the object surface. As the shape information of the object surface is carried by the deformed patterns, the 3D profile can be retrieved through analysing these patterns.

The phase unwrapping is a primary issue bound by the existing phase unwrapping techniques in FPP, aiming to recover the absolute phase from wrapped phase. The temporal phase unwrapping with multi-frequency fringe pattern was proposed, prominently advantaged by none-error propagation. Furthermore, the fringe order is deemed as the critical property to retrieve the absolute phase.

In Chapter 1, an overview of the 3D Profilometry is presented, which briefly introduce the Structured light technique, FPP, phase unwrapping and typical applications. Then, the problem statement and contribution elucidate the problems and achievements of this research, and following by lists the outline.

In Chapter 2, the thesis shall initially introduce the 3D FPP technique, inclusive of projection fringe analysis on FTP and PSP, existing phase unwrapping algorithms, e.g. spatial phase unwrapping and temporal phase unwrapping, computation of height information, and calibration. The proposed two-selected frequency projection fringe profilometry is introduced to retrieve the fringe orders with a corresponding

relationship, and calculate the absolute phase map with selected frequencies. Yet some impulsive errors shall remain when the fringe order map is being retrieved.

In Chapter 3, the experimental studies on the two-selected frequency projection fringe profilometry verify that the impulsive fringe order error (FOE) occurred when the surface contains discontinuities or separations, and these errors will affect the results of 3D reconstruction. Hence, the FOE correction is necessary.

In Chapter 4, a medium filter with selected parameters is proposed to remove the impulsive errors following two properties of fringe order, which are stepwise increase and impulsive property of FOEs. Subsequently, a framework to select sliding window size for medium filter is presented as a guideline for multiple situations. The experiment results prove that the proposed algorithm improves the accuracy of 3D reconstruction for objects.

Eventually, the conclusions, contributions, significance and the future work of this thesis shall be summarised.

Keywords: Fringe Projection Profilometry (FPP), Temporal Phase Unwrapping, Absolute Phase Maps, Multi-Frequency, Frequency Selection, Measurement range Analysis

CHAPTER 1: INTRODUCTION

1.1 Overview of 3D Profilometry

Over the past decades, the three-dimensional (3D) profilometry has been widely used in several areas, inclusive of computer vision, biomedical research, industrial applications, and virtual reality. Numerous techniques have been employed and improved for 3D profilometry, such as stereo vision [1-3], time-of-flight (TOF) [4, 5], and structured light [6, 7]. It can be classified into contact based techniques and non-contact techniques, and this thesis will focus on one of the non-contact techniques.

The non-contact techniques consist of passive techniques and active techniques. The stereo vision or computational vision is the main techniques of passive 3D profilometry. The TOF techniques or structured light techniques can be categorized into active 3D profilometry.

(a) Passive techniques

The stereo vision is a typical passive technique, which rely on ambient light and stereo cameras array to capture the images of the objects [1]. The stereo cameras array is employed to capture images from different angles, and then the inter-relationship, which is called relative difference or disparity, can be found from the two captured images. There, 3D shape of the object can be reconstructed. The stereo vision technique only requires the camera array to reconstruct the object, and it is provides a high-speed processing system. However, due to the using of two captured images that based on ambient light, the correspondence and reconstruction requires a long operational time [8]. Furthermore, the stereo vision technique is hard to reconstruct the objects that contains complex surface information, because the correspondence

processes will be inaccuracy [9]. Above all, the stereo vision technique has some limitations that restrict its application range.

(b) Active techniques

Compared with passive techniques above, the active techniques project a designed fringe pattern onto the object surface to reconstruct the 3D shape. Instead of taking advantages of texture and ambient light of the object, the active techniques use the deformed patterns to analyse the height information of the object, and then the after analysing the relationship between deformed patterns and projected patterns, the 3D shape can be reconstructed. The active techniques can be classified into two categories: TOF based active techniques [4, 5] and triangular geometry based structured light techniques [6, 7].

The TOF method requires a light source, a light sensor and a timer [4]. The pulsed modulated light source is used to project light, then the light sensor captures the reflected rays from the object, and the timer can calculate the time interval. The height information of the object can be measured by estimating the elapsed time, which is determined by the transmitting and receiving of time between light source and light sensor. However, the accuracy of TOF techniques are relatively low, because each point on the object surface must be projected. Therefore, the TOF method is time consuming.

The structured light techniques can be further classified into the Fringe projection profilometry (abbreviated as FPP) techniques or non-FPP techniques. FPP is one among the most frequently used approaches to retrieve 3D shape. This method shall project the sinusoidal patterns on the object surface and reference plane whereby a digital projector. On that basis, digital camera shall capture the reflected patterns deformed by the object surface. As the information of the object surface is carried by

the deformed patterns, the 3D profile can be retrieved through analysing these patterns. The details will be described in the following chapters.

1.1.1 Structured illumination in FPP

Structured light technique is a non-contact active system in FPP which project fringe patterns onto the object surface to retrieve the 3D shape of object. A traditional 3D FPP is illustrated with camera, projector, reference plane and object in Fig. 1.1.1. In the figure, l_0 defined as the distance between camera lens E_c and reference plane R, and d_0 expresses the distance between projector lens E_p and camera E_c, and height information of object is $h(\mathrm{x},\mathrm{y})$.

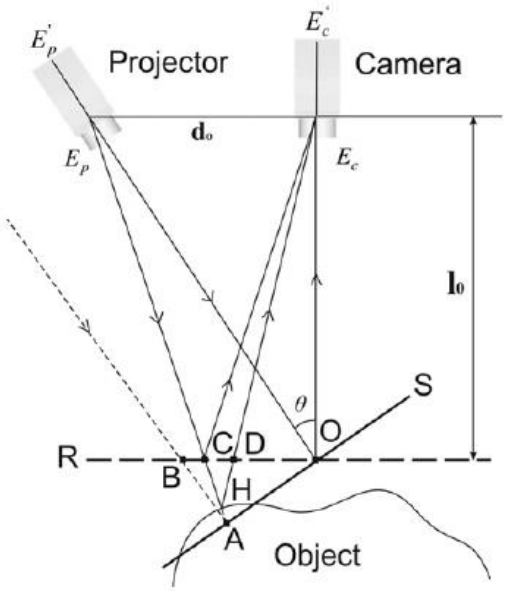

Fig. 1.1.1 Structured light System

First and foremost, the digital projector is employed to generate fringe patterns by computer which including sinusoidal patterns [10], binary patterns [11], triangular patterns [12] and other type of fringe patterns [13, 14] onto the reference plane. As the reference plane is removed, the identical fringe patterns shall be projected onto the object surface, and the projected fringes shall be simultaneously deformed because the

object changes stripes as modulation and deformed fringes carrying height information of object.

1.1.2 FPP

Among the foregoing operations, fringe analysis and phase unwrapping are the most significant steps to determine the phase maps.

Many approaches are developed to analyse the fringe patterns, among which the most frequently used to retrieve phase maps from fringe patterns, e.g. Moire technique (abbreviated as MT) [15], phase shift profilometry (abbreviated as PSP) or phase-measuring profilometry (abbreviated as PMP) [21], Fourier transform profilometry (abbreviated as FTP), modulation measurement profilometry (abbreviated as MMP) [16,17] and color-coded fringe projection [18,19]. The retrieved phase maps are ranging from $(-\pi, \pi)$ as wrapped, which are defined to be discontinuous and comprise steps of 2π. These wrapped phases fail to be directly used in 3D reconstruction. Therefore, the phase unwrapping approaches restore the absolute phase maps for these wrapped phases. Then, the phase difference can be obtained by subtracting deformed absolute phase map and reference absolute phase map. Finally, the height of object can be calculated. The steps are illustrated in the following Fig.1.1.2:

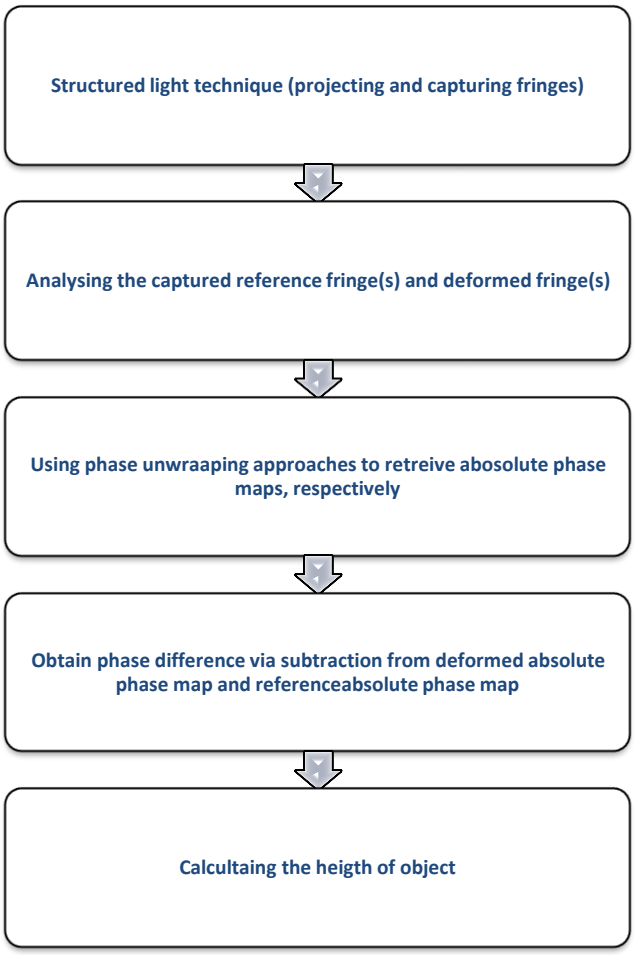

Fig. 1.1.2 Steps of FPP

The FPP techniques can be classified into single-shot technique and multiple-shot technique, which based on the number of used fringe patterns. The details will be introduced in Chapter 1.1.2.1 and 1.1.2.2.

1.1.2.1 Single-shot technique

The Single-shot technique such as FTP, color-coded fringe projection, saw-tooth FPP, frequency-coded pattern and stereo-vision which require only one reference pattern and one deformed pattern to retrieve the 3D object shape. Due to the advantage of fast calculation, the single-shot technique is suitable for moving object system.

(a) FTP

The FTP was proposed by Takeda et al. [22, 23], who transfer this method for signal processing techniques into the analysis of projection fringe to retrieve phase maps, and use the transformation of frequency to suppress the noise and high frequency harmonic components and other factors affecting the quality of phase map. The FTP is primarily advantaged by merely one reference image, and one deformed fringe pattern required to calculate wrapped phase. Acquisition speed of FTP outperforms that of other fringe analysis approaches. Nevertheless, several problems exist in FTP, inclusive of susceptibility of external optical conditions, ideal filter design, and slower calculation arising from Fourier transform and inverse Fourier transform. In this regard, it is of great necessity to seek out a stable and fast calculation for fringe analysis.

(b) Color-coded fringe projection

The Color-coded fringe projection composited by red, green and blue in the projector, and combined into one color-coded fringe pattern, which is projected onto the object surface [25-27]. A fringe pattern composed of sinusoidal stripes and color-coded stripes in a parallel placement, which generated by a projector with three independent acquisition channels for red, green and blue. The color-coded fringe pattern generated in the hue channel, and the different channels separate the different colours. In this way, the 3D reconstruction can be obtained. The color-coded fringe projection is a high speed technique and it is suitable for moving objects. However, the mutual interference of the different colour channels and extraction of colour stripes and sinusoidal fringes can severe impact the results of 3D reconstruction.

(c) Sawtooth fringe projection

The sawtooth fringe projection is a technique, which is only required one saw-tooth fringe pattern to reconstruct the 3D objects [14]. The liquid crystal display (LCD) projector projected saw-tooth stripes onto the object surface and captured by a digital camera. Then, the deformed pattern is converted to a wrapped phase map, and the quality-guided phase unwrapping algorithm retrieves the phase distribution without using any phase extract methods. Due to the use of one saw-tooth fringe pattern, the accuracy of the 3D reconstruction is affected by noises.

1.1.2.2 Multiple-shot technique

In contrast with the single-shot technique, the multiple-shot technique including PSP, binary coding profilometry method are basic with static object. These techniques require at least three fringe patterns to reconstruct the 3D shape of the object. Hence, the multiple-shot techniques are more robust than the single-shot techniques by employing more information to achieve efficient and accurate outputs.

(a) PSP

PSP is the most extensively studied and applied approach to analyse fringe proposed by Srinivasan, et al. [28]. In PSP, a bulk of shooting is required to acquire the image in stationary phase for references and objects, or to acquire fringe images being at least three phase-shifted to retrieve a phase map. Furthermore, to overcome the impact by noise and nonlinear distortion, PSP taking on four or *n* steps have also been studied and implemented [29]. Factoring in the trigonometric functions and the correlation of fixed phase shift fringes, the calculation has been expedited and simplified, and the quality of retrieved phase map have been optimised, in contrast to FTP. Nonetheless, more projected fringe images are required by PSP, prolonging the

acquisition of shooting. Additionally, the object is required to remain stationary, whereas phase errors are readily occurred in the calculation.

(b) Binary pattern technique

The binary pattern technique requires black and white stripes, which was generated with two illumination levels 0 and 1. The fringe pattern is divided into 2^n vertical stripes, and each fringe pattern consist of a unique binary code [30, 31]. The binary pattern technique is robust because of the characteristics of binary pattern (only generated by 0 and 1) to ambient light and the surface properties of the object. However, the binary patterns might generate ambiguities or errors on boundaries in the specific positions, and the acquisition time has been increased significantly because of the large sequence of binary patterns.

(c) Gray-level pattern technique

Instead of using two illumination levels to generate binary patterns, the gray-level pattern technique generates fringe patterns within multiple illumination levels, which highly increased the resolution of the measurement [32, 33]. A disadvantage is that, the gray-level pattern technique is easily influenced by reflected light from the object surface and it has ambiguity and unreliability to distinguish adjacent gray levels.

1.1.3 Phase unwrapping

The foregoing approaches are able to effectively analyse the phase maps of fringe patterns, whereas these wrapped phases fail to be directly used for 3D construction. In this regard, a major task bound by these techniques for phase analysis is perceived as the phase unwrapping, aiming to recover the absolute phase maps with continuous and discontinuous surfaces. The phase unwrapping methods can fall into

two categories, i.e. spatial phase unwrapping [34-37] and temporal phase unwrapping [38-41]. The spatial phase unwrapping counts as the earliest technology for phase unwrapping in projection fringe profilometry and for several applications. The quality-guided phase unwrapping (QGPU) technology [42, 43] is perceived as one among the most typical developed phase unwrapping method, aiming to unwrap a phase map through recovering the absolute phases along a certain path on the phase map from pixel with the highest quality to pixel with the lowest quality. Accordingly, the results of phase map could be confirmed, and meantime the impact by path selection on phase unwrapping shall be avoided. Yet this method remains dependent on the information of adjacent points to analysis the phase map, and subject to the problem of error propagation, that is, an error existing in a pixel shall affect the results of next pixel on the path [44, 45]. In the meantime, the requirements of real-time 3D reconstruction are hard to satisfy arising from the complex algorithms and longer computation of QGPU.

Given the requirements of high reliability, high speed and high accuracy, the researchers started to develop an algorithm to unwrap phase in the light of the projected multi-frequency fringes. Such algorithm shall project the digital fringe patterns taking on different spatial frequencies to the same object surface along the time axis for each independent pixel, i.e. the temporal phase unwrapping. As Huntley and Saldner [46] proposed, this approach is rapid and easy to calculate for single spatial frequency without information of adjacent points, the following path and propagating errors. As the developed technique for temporal phase unwrapping with multi-frequency fringe patterns in [47-50] indicates, with particular selected frequency, the results of phase unwrapping can be obtained independently taking on

different times and projection frequencies. In contrast to single frequency, the multi-frequency phase unwrapping algorithm can retrieve phase map accurately, rapidly and reliably whereby mathematical relationship between fringes and frequencies.

1.1.4 Applications of 3D Profilometry

As computer, optoelectronics and information processing technology advances, the digital projection-based FPP has been extensively used in industrial manufacture and test, medical engineering, security, entertainment and many other fields.

In industrial manufacture and test, to ensure the quality of the product, the precise 3D profilometry shall be employed for some complex surface, inclusive of turbine blades, preliminary configuration design for cars and aircrafts and ships. Comparatively, the traditional measurement technology is time consuming and imprecise. A structured-light system in car industry is introduced in publication [51, 52] for measuring the reconstruction information for a wheel rim and a car seat, which are shown in Fig 1.2.1 and Fig 1.2.2. The inspection conducted through this technique shall be collision-free, taking on an accuracy of 0.5mm on the object surfaces, and it is effective for curved surface object and even for discontinue surface.

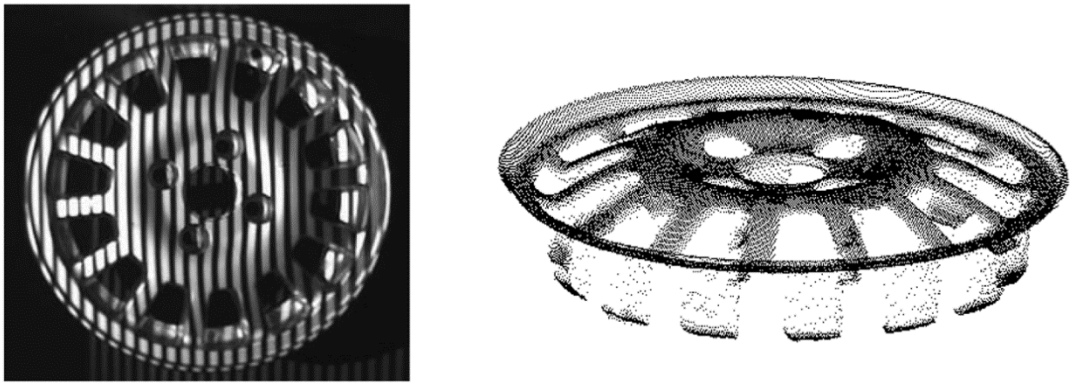

Fig. 1.2.1 Wheel Rim Measurement

Fig. 1.2.2 Structured-light 3D for a car seat

In medical engineering, 3D reconstruction technology can be used to measure body, simulate plastic surgery, design prosthesis, fulfil skin profilometry, map scleral lens, and to fulfil other medical applications. A skin profilometry technology [53] whereby a global facial image, and structured-light 3D system has been adopted practically. The 3D surface structure of human skin can be captured through adopting the dermaTOP instrument following digital fringe projection. Another novel technology refers to scleral lens mapping [54] shown in Fig. 1.2.3, which reconstructs the corneal and scleral surfaces whereby a reflection-based system taking on projected patterns.

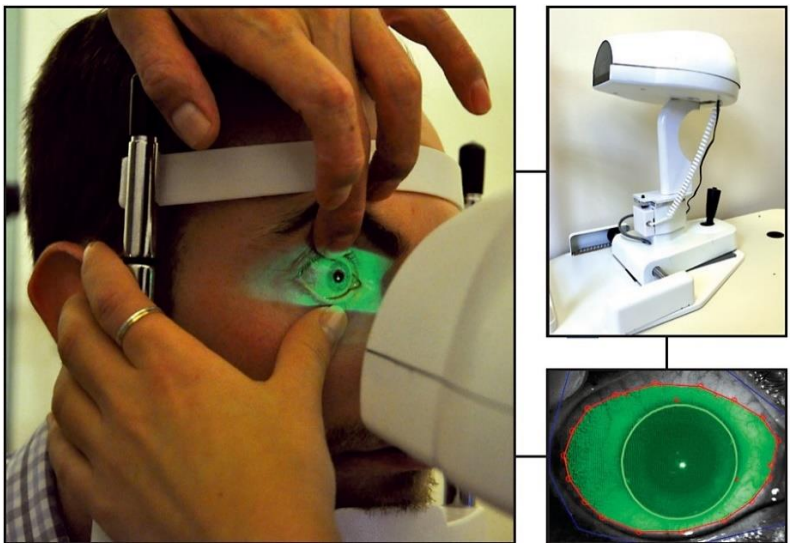

Fig. 1.2.3 Scleral Lens Mapping Instruments

In the field of security, 3D human feature recognition is employed to solidify national defence identify personnel, and it is effectuated in e-passport and visa application scenarios by virtue of the human characteristics. Wang, et al. [55], proposed a non-contact 3D fingerprint scan technology shown in Fig. 1.2.4 through which the fingerprint information can be precisely captured in 0.8s. Otherwise, there are another 3D recognition technology based on structured-light system, e.g. human ear recognition [56] and palmprint recognition system [57].

Fig. 1.2.4 Non-contact Fingerprint Scan

In entertainment and many other fields, inclusive of costume designing in Fig. 1.2.5, physical copies of cultural heritage, virtual reality, automatic parking system, and other areas, this approach has been extensively used. The ImMerge module and the ImEdit module of PolyWorks are adopted in costume designing where the 3D

reconstruction data can reach 233 μm in accuracy [51]; and an example is the reproduction at full scale of Winged Victory of Brescia [58] shown in Fig. 1.2.6; besides the 3D reconstruction brings accesses to didactical and visualisation purposes.

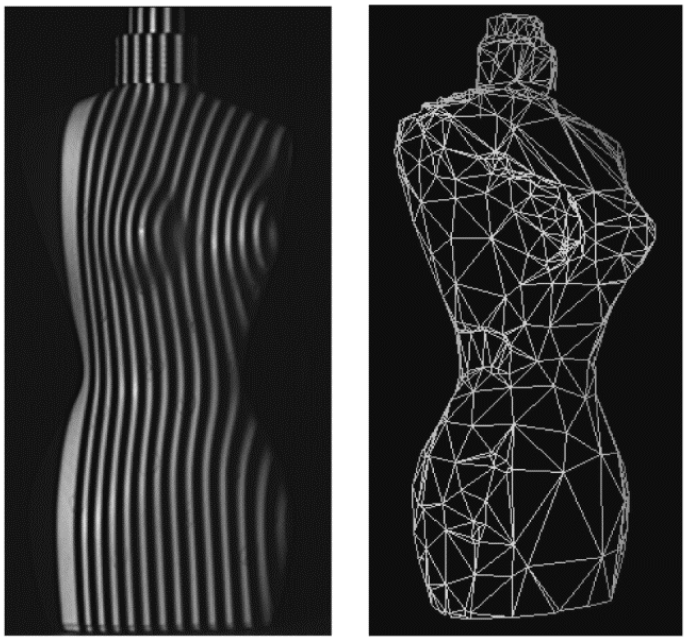

Fig. 1.2.5 Application in Costume Designing

Fig. 1.2.6 Physical Copies of Cultural Heritage

The non-contact 3D FPP based on digital fringe patterns has the strengths of non-contact, high speed, high accuracy and low cost. In recent years, this technology

has been paid more attention on researches and applications and has become one of the most important research direction.

1.2 Problem Statement

From the overview above, the FPP is one of the widely used technique for 3D reconstruction. The existing approaches and applications can retrieve 3D shape information with high accuracy, high resolution and fast speed, and foregoing unwrapping approaches could increase the performance of phase unwrapping efficiently. However, the phase errors remain when the wrapped phase maps are corrupted by evident noise and the object surface with discontinues or separations. The fringe order is the vital property of temporal phase unwrapping when retrieving 3D construction, and the impulsive noise could be denoted as fringe order error (FOE). The FOE shall be reflected in the retrieval results. For this reason, it is of critical significance for eliminating the FOE and studying on it. Yet there are some defects taken on by the existing researches.

1.3 Thesis Contributions

This thesis concentrated on fringe order impulsive errors correction using median filter for temporal phase unwrapping in FPP, which is a most popular issue in 3D profilometry. Two main issues concentrated on, including temporal phase unwrapping and fringe order impulsive errors using median filter.

The first issue is analysis method. The PSP and temporal phase unwrapping method are employed to gather shape information and measure height information of object. Using multi-frequency projection profilometry with look-up table method to calculate phase map. Then, FOE shall be focused.

Furthermore**,** a novel technique to correct the FOEs is proposed. Instead of using quality difference and increasing error bound, this method directly uses the monotonic increasing property of the fringe order sequence and the impulsive property taken on FOEs to recover the absolute phase map. Hence the reliability and efficiency of existing technique for temporal phase unwrapping shall be increased by this approach.

1.4 Thesis Outline

This thesis is comprised of five chapters. Each chapter is summarised below:

- Chapter 1 lays the overview of the 3D profilometry, elucidates the problem and contribution of this research, and lists the outline of the thesis.
- Chapter 2 reviews literatures of 3D fringe projection profilometry technique inclusive of FTP and PSP, fringe analysis, phase unwrapping algorithms, high computation, calibration and previous work.
- Chapter 3 shows experimental studies on the two-selected frequency projection fringe profilometry and discuss the FOE.
- Chapter 4 presents a novel technique for FOE analysis and correction in temporal phase unwrapping, and discusses the results of simulation and experiments.
- Chapter 5 emphasises the aim and contributions of the research project and sheds light on the significance of this research.

CHAPTER 2: 3D FRINGE PROJECTION PROFILOMETRY

2.1 Projection Fringe Analysis

Based on the existing digital fringe system, the approaches to analyse projection fringe, e.g. MT, PSP, FTP, modulation measurement profilometry (MMP), color-coded fringe projection, laser triangulation measurement, PMP and other approaches for fringe analysis, have been studied for several decades. These approaches basically solve the main problem existing in the fringe analysis and can retrieve the phase map from deformed pattern ranging from -π to π as wrapped. In this regard, high-precision approach to analyse fringe is required to unwrap the phase and reconstruct 3D for object surface.

2.1.1 Fourier Transform Profilometry

Among the foregoing fringe analysis approaches, the FTP can be completely used into high-speed measurement by virtue of its strengths, few images requirement to calculate wrapped phase, high accuracy and full-field analysis [59]. The patterns on the reference plane $G(x,y)$ and object $g(x,y)$ in FTP are described in following equations (2.1.1.1) and (2.1.1.2):

$$G(x,y) = \sum_{n=-\infty}^{\infty} b_r(x,y) A_n \exp(2i\pi nfx + \psi_k) \qquad (2.1.1.1)$$

and

$$g(x,y) = \sum_{n=-\infty}^{\infty} b_d(x,y) A_n \exp(i(2\pi nfx + n\varphi(x,y) + \psi_k)) \qquad (2.1.1.2)$$

where $b_r(x,y)$ and $b_d(x,y)$ are defined as reflectivity taken on by reference plane and object surface, and f is the projected fringe patterns with fixed frequency. $\varphi(x,y)$ denotes phase modulation result from the object height distribution. ψ_k expresses the

initial phase with harmonic components. It is possible to calculate phase difference between projected fringes on reference plane and object surface following Fourier-transform. As phase is unwrapped, the absolute phase difference can be retrieved. On that basis, the height information can be calculated.

The FTP is primarily advantaged by merely one reference fringe image and deformed fringe image required to calculate the phase map. It outperforms other approaches in the speed to acquire fringe image. Yet FTP itself is problematic, e.g. the susceptibility of external optical conditions and difficult design of ideal filter. When the projection signal reflectivity is different on reference plane and object surface, i.e. $b_r(x, y)$ and $b_d(x, y)$ are not a constant, the quality of the phase map attained by FTP shall be affected by the apparent reflection of reference plane, object and light conditions. In addition, the design of filter directly impacts on accuracy for the phase map. An approach was proposed by Su, *et al.* [60] to optimise FTP through adding a phase shift π. Nevertheless, the filter design problems and a bulk of fundamental problems remain insolvable. Accordingly, the approach to analyse fringe is required to be more accurate in further research.

2.1.2 Phase Shift Profilometry

PSP is proposed by Srinivasan, et al. [28], which need to capture a series of fixed fringe pattern with phase shift to calculate the phase map. In PSP, it is of critical significance for capturing a bulk of digital fringe patterns with fixed phase shift to acquire the phase map. To overcome the effects of noise, nonlinear distortion or other factors, at least three phase-shifted fringe patterns (three-steps PSP) are required for

reference plane and object to obtain the phase map. Moreover, the PSP based on four or more images has also been widely concerned and studied [61].

Fringe analysis in PSP calculates phase maps through employing the trigonometric functions, and the computer generates projection fringe patterns with $\frac{2\pi}{N}$ shift each phase shifting, where N defines the number of captured images (where N is a positive integer more than or equalling to 3). The fringe patterns are projected onto the reference plane and object surface, respectively. The equations of the reference fringes and the deformed fringes can be expressed as following:

$$\begin{cases} r_n(x,y) = I'_n(x,y) + I''_n(x,y)\cos\left[\omega(x,y) + 2\pi\frac{n}{N}\right] \\ d_n(x,y) = I'_n(x,y) + I''_n(x,y)\cos\left[\omega(x,y) + \Phi(x,y) + 2\pi\frac{n}{N}\right] \end{cases} \quad (2.1.2.1)$$

where $r_n(x,y)$ and $d_n(x,y)$ express the reference fringe and deformed fringe; $I'_n(x,y)$ denotes the intensity of ambient light and pattern offset, and $I''_n(x,y)$ indicates the intensity measured by amplitude of projected sinusoidal fringe patterns; $\omega(x,y)$ defines the phase value on reference plane, and $\Phi(x,y)$ is the phase difference retrieved through using a proper phase unwrapping approach with discontinued or separated surface. On that basis, the wrapped phase map $\phi_r(x,y)$ and $\phi_d(x,y)$can be retrieved as follows through adopting N-step PSP for reference plane and object plane, respectively:

$$\phi_r(x,y) = \arctan\left[\left(\frac{\sum_{n=1}^{N} r_n(x,y)\sin\left(2\pi\frac{n}{N}\right)}{\sum_{n=1}^{N} r_n(x,y)\cos\left(2\pi\frac{n}{N}\right)}\right)\right]$$

and (2.1.2.2)

$$\phi_d(x,y) = \arctan\left[\left(\frac{\sum_{n=1}^{N} d_n(x,y)\sin\left(2\pi\frac{n}{N}\right)}{\sum_{n=1}^{N} d_n(x,y)\cos\left(2\pi\frac{n}{N}\right)}\right)\right]$$

However, the wrapped phase maps cannot be used to obtain 3D reconstruction directly. Hence, the phase unwrapping techniques are necessary.

Through the foregoing equation series, the absolute phase maps for reference fringes and deformed fringes can be readily retrieved after phase unwrapping. Simultaneously, the absolute phase difference takes on the degree of modulation from the two captured fringe patterns on the object surface. This modulation involves the height information of the object. In this way, the 3D shape and height of the object can be accurately restored.

The impact by noise and other factors on the phase map is considerably mitigated by PSP through using multiple fixed phase-shift fringe images. Accordingly, the stability and accuracy of the calculation result can be evidently increased. Subsequently, in contrast to the previously frequently adopted Fourier profilometry, PSP merely requires simplified calculation, without Fourier transform or inverse transform, filter design or other complex operations. The calculation is markedly expedited. Furthermore, the reflection coefficient $I'_n(x, y)$ of the measured object surface is no effect on the calculated result in PSP. The attained phase map results are deemed accurate and stable.

Nevertheless, the main strength of PSP is the requirement for more projection fringe images, which increased the acquisition time, the shooting time and need to remain stationary for object. As acquired from the foregoing process, the PSP has been evident improved in contrast to FTP and effectuated in practical applications [55, 62, 63].

2.2 Phase unwrapping

According to the previously introduction of FTP and PSP techniques, the phase map could be retrieved. Yet to correctly reconstruct the 3D shape of object, it is of necessity to completely unwrap the phase on the retrieved phase map.

The fundamental phase unwrapping process is elucidated as the wrapped phase map in range $-\pi$ to $+\pi$, and adding or subtracting integer multiples of 2π. The results are able to be collected by the following equation:

$$\Phi(\mathrm{x},\mathrm{y}) = \phi(\mathrm{x},\mathrm{y}) + 2\pi\mathrm{k}(\mathrm{x},\mathrm{y}) \tag{2.2.1}$$

where $\Phi(x,y)$ denotes the unwrapped phase, $\phi(x,y)$ refers to the wrapped phase attained from Eq. (2.1.2.2), and $\mathrm{k}(x,y)$ is the integer number to represent fringe orders. Accordingly, the absolute phase can be attained clearly as the value of wrapped phase and fringe orders can be calculated precisely. In the light of the foregoing description, the typical wrapped phase map is obtained after analysing the projection fringe, and phase unwrapping approaches seek to retrieve the absolute phase map.

The existing methods to unwrap the phase are principally classified into two types shown in Fig. 2.2: 1. spatial phase unwrapping based on single frequency projection fringes; 2. temporal phase unwrapping technique based on multi-frequency projection fringes. The quality guided method (also known as path following method), Minimum-norm and other methods are involved in spatial phase unwrapping approach. Furthermore, the multi-frequency, multi-wavelength algorithms, and Gray-coded stripe are known as the approaches for temporal phase unwrapping.

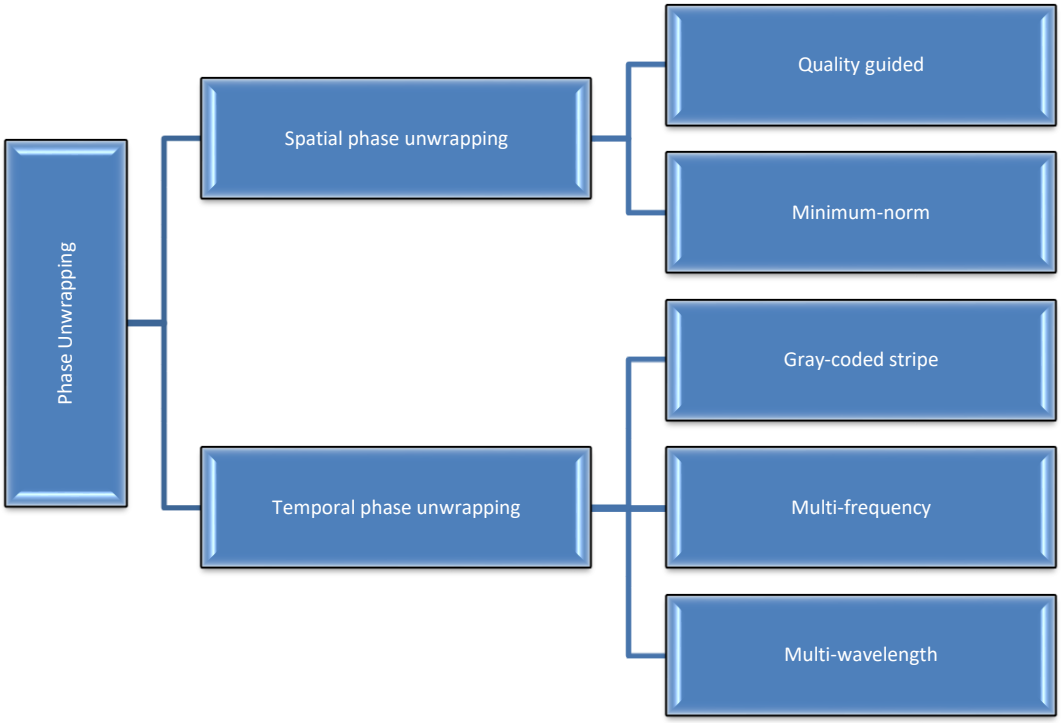

Fig. 2.2. Phase unwrapping

The spatial phase unwrapping approach counts as one among the technique for developed phase unwrapping, having been used in many areas, inclusive of geological exploration, remote sensing mapping and other applications. The temporal phase unwrapping approach is known as a novel technique for phase unwrapping having been developed in a decade characterised by high speed, high accuracy, and simple algorithm. Accordingly, the single frequency projection fringes-based spatial phase unwrapping technique and the multi-frequency projection fringes-based temporal phase unwrapping technique shall be primarily introduced in the following chapters.

2.2.1 Spatial Phase Unwrapping

The spatial phase unwrapping technique is known as one among the developed phase unwrapping approach in FPP. Several approaches for spatial phase unwrapping

with different considerations and requirements have been studied, inclusive of quality-guided method [64], Minimum-norm [65], Flynns method [66] and others [67].

Merely one spatial frequency of projection fringes is required by the spatial phase unwrapping technique to unwrap the phase. Basically, spatial phase unwrapping may be performed along the row or column of the phase matrix. As the phase map is retrieved, the method for spatial phase unwrapping is presented below: comparing the difference of adjacent two pixels relative to the phase value in the direction where phase is unwrapped, if the difference is less than $-\pi$, 2π shall be added on the latter point of the phase value; if the difference more than π, the phase value of latter pixel is required to subtract 2π. The absolute phase map is denoted as $\Phi_u(x,y)$, and the phase unwrapping process can be expresses as:

$$\Phi_u(x,y) = \phi_w(x,y) + 2\pi c(x,y) \tag{2.2.1.1}$$

where $\phi_w(x,y)$ defines wrapped phase values; $c(x,y)$ denotes wrap-count parameter which can be attained from the phase maps. On that basis, the object is assumed to be discontinued or separated in a pair of neighbouring pixels taking on the difference value over π. The differences can be eliminated through adding 2π on the measured phase value. Then, the phase can be readily unwrapped vertically and horizontally:

$$v(x,y) = \left\lfloor \frac{\phi_w(x,y) - \phi_w(x-1,y) + \pi}{2\pi} \right\rfloor$$

And (2.2.1.2)

$$z(x,y) = \left\lfloor \frac{\phi_w(x,y) - \phi_w(x,y-1) + \pi}{2\pi} \right\rfloor$$

where $v(x,y)$ and $z(x,y)$ expresses the unwrap phase values of vertical and horizontal direction; $\lfloor x \rfloor$ defines the largest integer of x. Subsequently, it is attained through incorporating Eq. (2.2.1.1) that:

$$v(x,y) = \mathrm{c}(\mathrm{x},\mathrm{y}) - \mathrm{c}(\mathrm{x}-1,\mathrm{y}) + \left\lfloor \frac{\phi_w(\mathrm{x},\mathrm{y}) - \phi_w(\mathrm{x}-1,\mathrm{y}) + \pi}{2\pi} \right\rfloor$$

and (2.2.1.3)

$$z(x,y) = \mathrm{c}(\mathrm{x},\mathrm{y}) - \mathrm{c}(\mathrm{x},\mathrm{y}-1) + \left\lfloor \frac{\phi_w(\mathrm{x},\mathrm{y}) - \phi_w(\mathrm{x},\mathrm{y}-1) + \pi}{2\pi} \right\rfloor$$

Based on these foregoing equations, the wrap-count parameter can be calculated vertically and horizontally from $\mathrm{c}(0,0)$ to $\mathrm{c}(\mathrm{x},\mathrm{y})$. The equation is expressed as:

$$\mathrm{c}(\mathrm{x},0) = \mathrm{c}(\mathrm{x}-1,0) + v(x,0) - \left\lfloor \frac{\phi_w(\mathrm{x},\mathrm{y}) - \phi_w(\mathrm{x}-1,\mathrm{y}) + \pi}{2\pi} \right\rfloor$$

and (2.2.1.4)

$$\mathrm{c}(\mathrm{x},\mathrm{y}) = \mathrm{c}(\mathrm{x},\mathrm{y}-1) + v(x,y) - \left\lfloor \frac{\phi_w(\mathrm{x},\mathrm{y}) - \phi_w(\mathrm{x},\mathrm{y}-1) + \pi}{2\pi} \right\rfloor$$

Accordingly, the wrap-count parameter of each pixel can be factored in, and absolute phase map is able to be calculated. In line with the above processes, the phase is required to be unwrapped for a two-dimensional array. Through summarising the calculation, the course is concluded as: first and foremost, unwrap the phase along a vertical direction of two-dimensional data array (the first column can be generally selected); secondly, establish unwrapped phase value of this column as a benchmark; finally, unwrap the phase horizontally to distribute the 2D absolute phase map. It is the simplest and most commonly adopted approach for spatial phase unwrapping. The main strength taken on by this method is simple and fast.

Nevertheless, in the problem of 3D profilometry measurement of a complex object, the deformed patterns turn out to be excessively complicated. This primarily arises from the large fluctuation on the object surface, inclusive of noise effects, shadows, fringe discontinues, and pixel sampling problem (phase difference between adjacent two sampling points may be more than π or less than $-\pi$). In this regard, if the phase unwrapping remains to be performed through adopting this method, the different selection of the path is found to generate different results in phase unwrapping. In other words, the result of this spatial phase unwrapping method is path dependent. Besides, if the selected path is inconsistent, it may arouse inconsistencies in the results of phase unwrapping, and results of phase unwrapping are erroneous to retrieve the 3D shape.

To optimise the path dependence, researchers have proposed some phase unwrapping algorithms to improve the accuracy. The quality-guided method is a representative algorithm for spatial phase unwrapping, which is to estimate the correctness of phase value at each pixel based on a new parameter, and then set the modulation intensity threshold to determine the correct pixels. On that basis, the phase unwrapping process can acquire the correct results. The quality-guided method is advantageous in: the results of phase unwrapping can be retrieved whereby pixels taking on better quality other than data with poor quality resulting from the selected area. The quality-guided method outperforms the foregoing methods, while it remains dependent on the information of adjacent points for analysis and calculation. In the meantime, the complex algorithm and the longer computation time also make it difficult for spatial phase unwrapping to real-time acquire the 3D profilometry.

2.2.2 Temporal Phase Unwrapping

In contrast to spatial phase unwrapping, a novel technique named temporal phase unwrapping, not depending on the expansion path and adjacent pixel information, being accurate and rapid, was presented to solve the problem for objects taking on separations and discontinuities. As found by Huntley and Saldner [46] through adopting fringes taking on multiple frequencies along the time axis to acquire phase information, the phase unwrapping depends no longer on adjacent point information and path. On that basis, they proposed the multi-frequency projection fringes-based technique for temporal phase unwrapping. The key of this technique is that the different frequency patterns are projected onto the object surface at different times, and the frequencies of these fringe patterns are selected and designed to ensure that a unique result of phase unwrapping.

A fringe pattern is assumed to be projected at time $t;$ and another different spatial frequency pattern is assumed to be projected at time $t-1$; the wrapped phase map is defined as $\phi_w(\mathrm{x},\mathrm{y},\mathrm{t})$ along the time axis ($t = 0,1,2,3 \dots s$). Accordingly, the phase different $\Delta\phi_w(\mathrm{x},\mathrm{y},\mathrm{t})$ for wrapped phase map can be attained as:

$$\Delta\phi_w(\mathrm{x},\mathrm{y},\mathrm{t}) = \phi_w(\mathrm{x},\mathrm{y},\mathrm{t}) - \phi_w(\mathrm{x},\mathrm{y},\mathrm{t}-1) \tag{2.2.2.1}$$

The phase discontinuities (whether larger or less than 2π) at time t and $t-1$ can be calculated with through dividing 2π, and an integer operator is presented below:

$$d(\mathrm{x},\mathrm{y},\mathrm{t}) = \frac{\Delta\phi_w(\mathrm{x},\mathrm{y},\mathrm{t})}{2\pi} \tag{2.2.2.2}$$

Besides, phase discontinuities of first pixel $\Phi_1(x,y,s)$ are expressed as:

$$\Phi_1(\mathrm{x},\mathrm{y},\mathrm{s}) = d_1(\mathrm{x},\mathrm{y},\mathrm{t}) \tag{2.2.2.3}$$

Thus, the phase discontinuities $\Phi_s(\mathrm{x},\mathrm{y},\mathrm{s})$ at time s can be summarised from time of 1 to s without further phase unwrapping:

$$\Phi_s(\mathrm{x},\mathrm{y},\mathrm{s}) = \sum_{t=1}^{s} d(\mathrm{x},\mathrm{y},\mathrm{t})$$

The absolute phase value of each pixel, can be accurately determined by this approach, and the entire absolute phase map can be attained.

As acquired from the foregoing calculation, the operation for each pixel of temporal phase unwrapping algorithm is independent. The absolute phase values of each pixel are calculated independently following the pixel information along the time axis, and the path dependence is solved in phase unwrapping. Simultaneously, the temporal phase unwrapping is simple and fast compared with the technique of spatial phase unwrapping, and efficiency has been remarkably optimised.

Certainly, more data is required by the temporal phase unwrapping approach than other unwrapping algorithms. Basically, the PSP required at least three of the deformed fringe images and reference fringe patterns for each spatial frequency. In this regard, the total amount of projected fringe pattern is large, and this shall consume excessive time for capturing and analysing fringe images though the calculation has been expedited. The following Chapters shall describe the subdivisions with Gray code algorithm, Multi-frequency temporal phase unwrapping and Multi-Wavelength Temporal Phase Unwrapping.

2.2.2a Gray-Coded Stripe

Coded structured light system is one among the most extensively adopted techniques to retrieve the height information of object, inclusive of Gray coded stripe

algorithm with phase shifting [68-70], binary coding [71, 72], *n*-ary codes [73], hybrid techniques [74, 75] and other algorithms [76]. The Gray code algorithm takes on some strengths on codification, e.g. punctually pixel codification and unnecessity to consider spatial neighbourhood.

The key of Gray code algorithm is to project some Gray coded patterns onto the object surface to label the measurement areas with corresponding sinusoidal patterns, and the sinusoidal patterns are denoted by grey levels. The sinusoidal patterns are projected on the object surface taking on four-step phase shifting periodic intensity patterns, which are expressed below:

$$I_n(x,y) = a(x,y) + b(x,y)\cos(\phi_G(x,y) + \phi_n) \qquad (2.2.2a.1)$$

where $I_n(x,y)$ denotes projected patterns intensity; $a(x,y)$ refers to the intensity of background; $b(x,y)$ defines the intensity modulation; $\phi_G(x,y)$ is the wrapped phase for Gray coded stripe and ϕ_n indicates phase shift with four-step phase shift technique with n equalling from 1 to 4. Accordingly, the wrapped phase for each certain point on surface can be precisely calculated:

$$\phi_G(x,y) = \arctan\left(\frac{I_2(x,y) - I_4(x,y)}{I_3(x,y) - I_1(x,y)}\right)$$

The phase value shall be wrapped into [-π, π]. The number of code words is equal to the number of periods of projected fringe patterns when the traditional Gray-code is being encoded. The traditional Gray-code patterns are defined as $log_2 N$, where N denotes code words number.

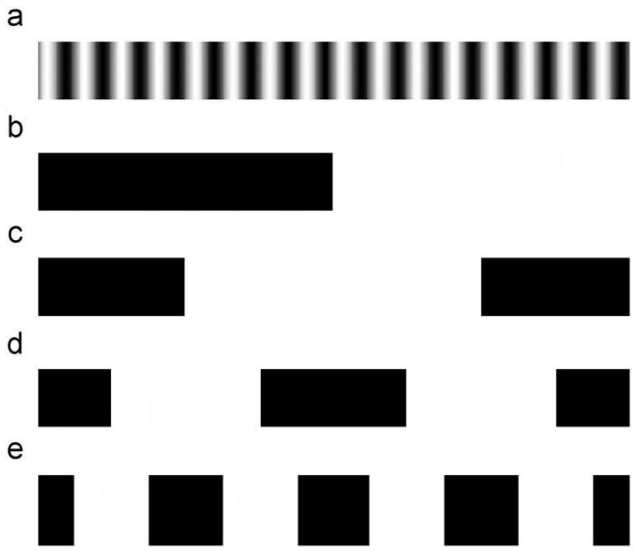

Fig. 2.2.2a (a) one of projected sinusoidal pattern (b) –(e) traditional Gray-code patterns

The Fig. 2.2.2a (a) illustrates the number of phase-shift pattern which equals to 16, i.e. the number of *N*. Hence, there are four Gray-code patterns, i.e. G_1, G_2, G_3, and G_4 can be calculated as Fig. 2.2.2a (b) to (e), and associated with a decimal number *D* defined below:

$$\mathrm{D} = \sum_{i=0}^{n-1} G_i \cdot 2^{n-i}$$

where n defines the number of Gray-code patterns. On that basis, the fringe order $k_h(x, y)$ can be determined through corresponding decoding results as an example:

Codes words	c_0	c_1	c_2	c_3	c_4	c_5	c_6	c_7	c_8	c_9	c_{10}	c_{11}	c_{12}	c_{13}	c_{14}	c_{15}
D	0	1	3	2	6	7	5	4	12	13	15	14	10	11	9	8
k_h	0	1	2	3	4	5	6	7	8	9	10	11	12	13	14	15

Table 2.2.2a the corresponding relationship of fringe order and Gray-code words

The absolute phase map can be completely retrieved whereby this algorithm. Nevertheless, there are some weaknesses taken on by Gray cade algorithm, inclusive

of the discrete property of Gray cade patterns restricts the resolution, ambiguity in determination of the projected patterns which captured by camera, and errors shall be readily triggered by the calculation.

2.2.2b Multi-frequency temporal phase unwrapping

The multi-frequency temporal phase unwrapping was proposed in [46] initially. In this method, the fringe patterns taking on different fringe densities are projected onto the object, and the deformed fringe patterns are captured. Through using N-step method, a coarsest fringe patterns taking on low frequency can be referenced to unwrap the phase, with the values confined into [-π, π]. The wrapped phase maps measured by high frequency shall be unwrapped one by one based on previous phase maps.

The key of multi-frequency temporal phase unwrapping is to employ a low frequency and a high frequency, which '*l*' and '*h*' are assumed for subscripts, respectively. In line with the previous work, it is easy to prove that the two phase maps should be related to each other below:

$$\Phi_h(x,y) = \left(\frac{\lambda_l}{\lambda_h}\right)\Phi_l(x,y) \tag{2.2.2b.1}$$

In this regard, based on Eq. (2.2.2b.1), the phase maps ($\Phi_h(x,y)$ and $\Phi_l(x,y)$) are related, and how the wrapped phase maps ($\phi_h(x,y)$ and $\phi_l(x,y)$) are associated can be expressed as:

$$\begin{cases} \Phi_h(x,y) = \phi_h(x,y) + 2\pi k_h(x,y) \\ \Phi_l(x,y) = \phi_l(x,y) + 2\pi k_l(x,y) \end{cases} \tag{2.2.2b.2}$$

where the $k_h(x,y)$and $k_l(x,y)$ refers to the integer fringe orders, respectively. The

low-resolution phase distribution $\phi_l(x,y)$ is provided by low frequency fringe through drawing upon unit frequency patterns. Subsequently, the fringe order $k_h(x,y)$ for each pixel can be determined readily through incorporating Eq. (2.2.2b.1) and (2.2.2b.2):

$$k_h(x,y) = int\left[\frac{\left(\frac{\lambda_l}{\lambda_h}\right)\Phi_l(x,y) - \phi_h(x,y)}{2\pi}\right] \tag{2.2.2b.3}$$

where int[a] is to acquire the closest integer value of a. In this way, the high frequency phase $\Phi_h(x,y)$ could be unwrapped via fringe order $k_h(x,y)$.

2.2.2c Multi-Wavelength Temporal Phase Unwrapping

An alternative phase unwrapping approach is a multi-wavelength temporal phase unwrapping algorithm. This technique is conducive to resolving phase discontinuities. A synthetic wavelength is used as a reference to unwrap the phase maps, which is expressed as:

$$\lambda_{eq} = \frac{\lambda_l \lambda_h}{\lambda_l - \lambda_h} \tag{2.2.2c.1}$$

where the λ_{eq} refers to equivalent wavelength. By and large, the synthetic wavelength can be adequately large to eliminate the phase ambiguity as the measurement range rises through sacrificing its signal to noise ratio (SNR). For this reason, the synthetic phase map ϕ_{eq} is commonly selected to assist phase unwrapping. A factor used to determine fringe order with a more sensitive wavelength is a proportion $\frac{\lambda_{eq}}{\lambda_h}$ of the synthetic wavelength and original wavelength:

$$k_h(x,y) = int\left[\frac{\left(\frac{\lambda_{eq}}{\lambda_h}\right)\Phi_{eq}(x,y) - \phi_h(x,y)}{2\pi}\right] \tag{2.2.2c.2}$$

It is noteworthy that the two-wavelength temporal phase unwrapping method can be increased and the unambiguous measurement range can be maximised abiding by an optimisation criterion leading to a geometric series of wavelengths.

2.2.3a Two Selected Frequency Projection Fringe Profilometry

Multi-frequency projection fringe profilometry has great worth to research and application, especially in calculation speed and results stability. Yet the traditional multi-frequency projection fringe technology needs to collect too many projected fringe images, which shall evidently reduce the efficiency of 3D data acquisition. A proposed two-selected frequency projection fringe technique uses less projected fringe images to ensure measurement accuracy, meet the requirements of high-precision for real-time measurements and fast calculation [77, 78].

The spatial frequencies of the projected fringe are defined as f_l and f_h, respectively for low frequency and high frequency, i.e. the number of fringes on the projected pattern. On that basis, two selected frequencies are projected onto the object surface, and the deformed patterns can be captured as $d_h(x,y)$ and $d_l(x,y)$, respectively:

$$\begin{cases} d_h(x,y) = A(x,y) + B(x,y)\cos[\Phi_h(x,y)] \\ d_l(x,y) = A(x,y) + B(x,y)cos[\Phi_l(x,y)] \end{cases} \quad (2.2.3.1)$$

where (x,y) denotes each pixel on the coordinates of the projected fringe image; $A(x,y)$ refers to the intensity of background light; $B(x,y)$ denotes the intensity of the projected fringes; $\Phi_h(x,y)$ and $\Phi_l(x,y)$ are the absolute phase maps. Yet the wrapped phase $\phi_h(x,y)$ and $\phi_l(x,y)$ can be only retrieved by analysing deformed patterns. Hence, how wrapped phase and unwrapped phase are related is indicated below:

$$\begin{cases} \phi_h(x,y) = \Phi_h(x,y) - 2\pi k_h(x,y) \\ \phi_l(x,y) = \Phi_l(x,y) - 2\pi k_l(x,y) \end{cases} \quad (2.2.3.2)$$

where $k_h(x,y)$ and $k_l(x,y)$ refer to the integer fringe order for two selected frequencies. Then, the algorithms to unwrap the phase are summarised as:

$$\begin{cases} \Phi_h(x,y) = \phi_h(x,y) + 2\pi k_h(x,y) \\ \Phi_l(x,y) = \phi_l(x,y) + 2\pi k_l(x,y) \end{cases} \quad (2.2.3.3)$$

From Eq. 2.2.3.3, it can be seen that if seeking to reach an accurate result of phase unwrapping, the correct number of fringe order *k* shall be factored in. The traditional technique to unwrap the spatial phase merely determines these integers through drawing upon the relationship between adjacent pixels. The result of spatial phase unwrapping is susceptible to the adjacent pixels and tends to trigger error propagation. Temporal phase unwrapping technology analyses the same pixel at different times and frequencies of projected patterns for calculation. In this regard, it shall not propagate the error, and the reliability and stability have been evidently increased.

The phase map $\phi_h(x,y)$ and $\phi_l(x,y)$ can be measured according to the foregoing algorithm, whereas $\Phi_h(x,y)$, $\Phi_l(x,y)$, $k_h(x,y)$ and $k_l(x,y)$ are required to be factored in. In line with the relationship in [33], the following expression can be derived:

$$f_l \cdot \phi_h(x,y) = f_h \cdot \phi_l(x,y) \quad (2.2.3.4)$$

Accordingly, through incorporating the Eq. (2.2.3.3) and (2.2.3.4), a relationship is attained as:

$$\frac{f_l\phi_h(x,y) - f_h\phi_l(x,y)}{2\pi} = k_l(x,y)f_h - k_h(x,y)f_l \quad (2.2.3.5)$$

As the above expression indicates, the fringe order of each selected frequency pattern $k_h(x,y)$ and $k_l(x,y)$ is solvable. This is because the right side of equation is an

integer. Similarly, the left side must also be an integer. The corresponding relationship for both side can be readily acquired from the analysis results for $\phi_h(x,y)$ and $\phi_l(x,y)$, and selected frequencies f_h and f_l. In this regard, the fringe order $k_h(x,y)$ and $k_l(x,y)$ can be calculated with:

$$k_h(x,y)=\begin{cases} int[\frac{f_h}{2}] & [f_h-(f_h mod 2+1)]\pi \le f_h\Phi_h(x,y) < f_h\pi \\ \cdots & \cdots \\ 1 & \pi \le f_h\Phi_h(x,y) < 3\pi \\ 0 & -\pi \le f_h\Phi_h(x,y) < \pi \\ -1 & -3\pi \le f_h\Phi_h(x,y) < -\pi \\ \cdots & \cdots \\ -int[\frac{f_h}{2}] & -f_h\pi < f_h\Phi_h(x,y) \le -[f_h-(f_h mod 2+1)]\pi \end{cases} \quad (2.2.3.6)$$

and

$$k_l(x,y)=\begin{cases} int[\frac{f_l}{2}] & [f_l-(f_l mod 2+1)]\pi \le f_l\Phi_l(x,y) < f_l\pi \\ \cdots & \cdots \\ 1 & \pi \le f_l\Phi_l(x,y) < 3\pi \\ 0 & -\pi \le f_l\Phi_l(x,y) < \pi \\ -1 & -3\pi \le f_l\Phi_l(x,y) < -\pi \\ \cdots & \cdots \\ -int[\frac{f_l}{2}] & -f_l\pi < f_l\Phi_l(x,y) \le -[f_l-(f_l mod 2+1)]\pi \end{cases} \quad (2.2.3.7)$$

where $[x]$ denotes the integer, not surmounting x. Nevertheless, the absolute phase map $\Phi_h(x,y)$ and $\Phi_l(x,y)$ fail to determine the fringe order $k_h(x,y)$ and $k_l(x,y)$ directly when phase is being unwrapped. There, a normalised spatial frequency $f_0=1$ is established to define the wrapped phase map $\phi_0(x,y)$ and absolute phase map $\Phi_0(x,y)$ for corresponding relationship for $\Phi_h(x,y)$ and $\Phi_l(x,y)$:

$$\Phi_h(x,y)=f_h\cdot\Phi_0(x,y) \quad (2.2.3.8)$$

and

$$\Phi_l(x,y)=f_l\cdot\Phi_0(x,y) \quad (2.2.3.9)$$

Incorporate the Eq. (2.2.3.6), (2.2.3.7), (2.2.3.8) and Eq. (2.2.3.9), when the $k_l(x,y)f_h - k_h(x,y)f_l$ and the range of absolute phase $\Phi_0(x,y)$ are determined, the fringe order $k_h(x,y)$ and $k_l(x,y)$ can be calculated independently.

To summarise the foregoing algorithms, the process can be concluded below:

1. Select two frequencies f_h and f_l (integer) and attain the deformed patterns for each frequency. On that basis, match the relationship of $k_l(x,y)f_h - k_h(x,y)f_l$ and $k_l(x,y)$, $k_h(x,y)$.
2. Project fringes of these two frequencies onto the object surface and measure the phase map $\phi_h(x,y)$ and $\phi_l(x,y)$ through adopting technique of fringe analysis.
3. Calculate $\frac{f_l\phi_h(x,y) - f_h\phi_l(x,y)}{2\pi}$, and select the nearest integers. On that basis, match each integer with $k_l(x,y)f_h - k_h(x,y)f_l$ and select the nearest value for $k_l(x,y)$ and $k_h(x,y)$, respectively.
4. Adopt the fringe order $k_l(x,y)$ and $k_h(x,y)$ to retrieve the absolute phase map of the two selected frequency fringes.

As the above steps, this approach is able to retrieve the absolute phase map correctly, and merely two selected frequency fringes are adopted. Compared with existing techniques for temporal phase unwrapping, this approach shall substantially reduce the required number of projection images and ensures the measurement to be accurate simultaneously.

2.2.3b Frequency selection for Two Frequency Projection Fringe Profilometry

As the background shown above, two selected spatial fringe patterns are projected onto the object surface as f_h and f_l, and the frequency f_h surmounts f_l. Given the sinusoidal variation property, the phase unwrapping algorithms can be adopted to attain absolute phase map whereby a corresponding relationship:

$$\frac{f_l\phi_h(x,y) - f_h\phi_l(x,y)}{2\pi} = k_l(x,y)f_h - k_h(x,y)f_l$$

Accordingly, the f_h and f_l can be used to acquire the fringe orders, the wrapped phase value $\phi_h(x,y)$ and $\phi_l(x,y)$ should be attained from fringe analysis.

From foregoing operations, this corresponding relationship counts as the most crucial section to seek the one-one correspondence from $\frac{f_l\phi_h(x,y)-f_h\phi_l(x,y)}{2\pi}$ to fringe order $k_l(x,y)$ and $k_h(x,y)$. Yet the selection of two selected spatial fringe patterns is to ensure the existence of the one-one correspondence. As the analysis of selection indicates in [77, 78], when normalised spatial frequency $f_0 = 1$, the range of absolute phase map $\Phi_0(x,y)$ shall be discussed. From Eq. (2.2.3.6), the range of absolute phase map for high frequency can fall into N sections, where $N = 2\left[\frac{f}{2}\right] + 1$, and interval boundaries for each interval is denoted as $\frac{(2\mathrm{n}+1)\pi}{f}$, where $-\mathrm{int}\left[\frac{f}{2}\right] < \mathrm{n} < \mathrm{int}\left[\frac{f}{2}\right]$. On that basis, different value can be obtained by the fringe order at each interval. The analysis is similar to that on the low frequency. In this regard, it is evident that the interval boundaries for each interval is distinctive, and the corresponding relationship and fringe order are unique when f_h and f_l are pairwise coprime ($\frac{(2\mathrm{n}_h+1)\pi}{f_h} \neq \frac{(2\mathrm{n}_l+1)\pi}{f_l}$). Yet if the f_h and f_l is not pairwise coprime, $\frac{(2\mathrm{n}_h+1)\pi}{f_h} = \frac{(2\mathrm{n}_l+1)\pi}{f_l}$ shall be satisfied. In other words, as monotonicity for $\Phi_0(x,y)$ rises, each fringe order $k_l(x,y)$ and $k_h(x,y)$ shall be incorporated on unique (x,y) on $\Phi_0(x,y)$,

respectively. In this regard, the following statements are proposed to select the frequencies:

Statement 1: the phase map of these selected frequencies can fall into several intervals based on pixels (x, y) as the selected frequencies f_h and f_l is pairwise coprime; the fringe order $k_l(x, y)$ and $k_h(x, y)$ shall be incorporated distinctively at each interval; accordingly, the absolute phase map can be retrieved whereby these attained values of fringe order.

Statement 2: as the selected frequencies f_h and f_l are pairwise coprime, any two different intervals of two selected frequencies shall have two corresponding combinations complying with statement 1 and should satisfy conditions below:

$$\frac{f_l\phi_h(x_a, y_a) - f_h\phi_l(x_a, y_a)}{2\pi} \neq \frac{f_l\phi_h(x_b, y_b) - f_h\phi_l(x_b, y_b)}{2\pi}$$

or

$$k_l(x_a, y_a)f_h - k_h(x_a, y_a)f_l \neq k_l(x_b, y_b)f_h - k_h(x_b, y_b)f_l$$

where (x_a, y_a) and (x_b, y_b) denote different intervals. In other words, fringe order and $\frac{f_l\phi_h(x,y)-f_h\phi_l(x,y)}{2\pi}$ are distinctively and correspondingly related.

Statement 3: if the selected frequencies f_h and f_l are pairwise coprime, each value of $\frac{f_l\phi_h(x,y)-f_h\phi_l(x,y)}{2\pi}$ shall have a distinctive mapping corresponding to values of fringe order, which can be adopted to unwrap the phase.

To sum up the above discussion, the frequency selection-based two-frequency projection algorithm is comparatively common, and as the proposed statements indicate, the frequency selection combinations that can be selected by people to

increase phase unwrapping substantially. These general rules also present an aim to select multiple frequencies to increase the capability to resist phase error. The theory and practice are of critical significance for studying the two-frequency projection profilometry.

2.3 Fringe order errors

The key for accurate phase unwrapping is to obtain correct fringe order for each pixel in the phase map. In ideal cases of free noise and continuous surfaces, the process is simple and straightforward, but fringe order errors may still occur in practice. Ideally, the fringe order sequence should exhibit a step-wise increase with respect to the direction vertical to the fringes (i.e., x-axis) and step height should always be 1. However, when the surface contains steps or discontinuities, the fringe order sequence will be corrupted by impulsive errors. The following figure is the fringe order of an unwrapped phase map obtained in our laboratory for an object with steps on the surface. Note that these errors are impulsive because the errors do not propagate to adjacent pixels. Hence, the fringe order errors may occur in three situations (shown as figure):

1. The single pixel fringe order error appears as a one-pixel pulse in the fringe order map in time t.
2. Multiple successive pixels are corrupted by fringe order errors (t, t+N).
3. The fringe order errors may also occur on the boundary of adjacent fringes. In other word, the fringe order error will be coincided with the step-wise increase.

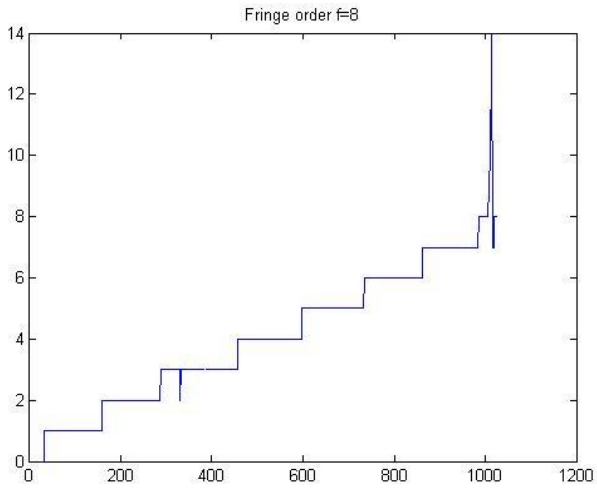

Fig. 2.3. Example for a fringe order with impulsive errors

2.4 Height Computation

According to the above phase unwrapping processes, the unwrapped phase values can be retrieved. The unwrapped phase maps $\Phi_{hr}(x,y)$ and $\Phi_{hd}(x,y)$, and $\Phi_{lr}(x,y)$ and $\Phi_{ld}(x,y)$ for reference plane and deformed plane are determined, which calculated from wrapped phase maps, respectively. Then, the absolute phase difference can be calculated as following:

$$\Delta\,\Phi_l(x,y) = \Phi_{ld}(x,y) - \Phi_{lr}(x,y) = 2\pi k f_0 \overline{CD} \qquad (2.3.1)$$

where $\Delta\,\Phi_l(x,y)$ defines absolute phase difference. In this regard, the height information of measured object can be determined from the triangular relationship of the Structured light system. As shown Fig. 1.1.1, a fringe pattern generated by the projector is projected on the reference plane and reflect to the camera at point C. While, when the reference plane is withdrawn, the same fringe pattern is reflected to the camera at point H via point D on the reference plane. The ΔHCD and ΔHE_pE_c are similar triangles. Hence, we have:

$$\frac{\overline{CD}}{d_0} = \frac{-h(x)}{l_0 - h(x)} \qquad (2.3.2)$$

Then, we combie the Eq. (2.3.1) and Eq. (2.3.2). In this regard, the height information of measured object can be determined from the triangular relationship of the system with the difference between unwrapped phases:

$$h(\mathrm{x},\mathrm{y}) = \frac{l_0 \Delta\, \Phi_l(x,y)}{\Delta\, \Phi_l(x,y) - 2\pi f_0 d_0} \tag{2.3.3}$$

The same operation can be used to retreive height information with high frequency. From the above equations, it can be seen that when the phase difference is obtained, the height informatin of object can be retrieved.

2.5 Calibration

As described above, the structured light system employees a camera and a projector to reconstruct 3D shape of object. The accuracy of the system is more essential, which can be affected by many factors such as the parameters of system devices, and the spatial frequency for fringe patterns. Hence, a proper calibration method can achieve the accurate reconstruction of 3D shapes. The methods based on neural networks [79], bundle adjustment [80] and absolute phase [81] have been researched.

Zhang and Huang [82], which the projector is set as an inversed camera, proposed the calibration system. The calibration for the projector is the same as the camera. In the method, the calibration is fast, robust, and accurate, and projector can be calibrated by a stereo vision system similar with camera calibration. The calibration details for this thesis will be discussed in the Experiment set-up.

2.6 Conclusion

The two most crucial sections of 3D reconstruction, i.e. projection fringe analysis methods and phase unwrapping techniques, are discussed in the light of the projected

fringe patterns. Among the approaches to analyse the projection fringe, the FTP and PSP have been recommended and analysed. The phase unwrapping techniques principally lay the stress on the spatial phase unwrapping on the basis of single frequency pattern and the temporal phase unwrapping in line with multiple frequencies patterns, especially for temporal phase unwrapping, inclusive of Gray code method, multi-frequency temporal phase unwrapping, multi-wavelength temporal phase unwrapping and two-selected frequency projection fringe technique. After phase unwrapping, the height information of object can be retrieved. In Chapter 2.4, a brief introduction of calibration is given. These introductions and discussions lay the fundamental knowledge and motivate the following research.

CHAPTER 3: EXPERIMENTAL STUDIES ON THE TWO SELECTED FREQUENCY PROJECTION FRINGE PROFILOMETRY

3.1 Experiment set-up

In this section, the experiment set-up for this thesis is provided and based on the measurement system for fringe projection profilometry. A Dalsa Genie HM1024 high-resolution digital camera with 1024-pixel × 768-pixel resolution and Acer Led CWX1147 1280-pixel × 1024-pixel projector are adopted in this experiment as devices, and the system, camera and projector are presented in Fig. 3.1.1. The distance from the reference plane to the camera lens l_0 is 1000mm, and the distance from the camera lens to the projector lens d_0 is 200mm.

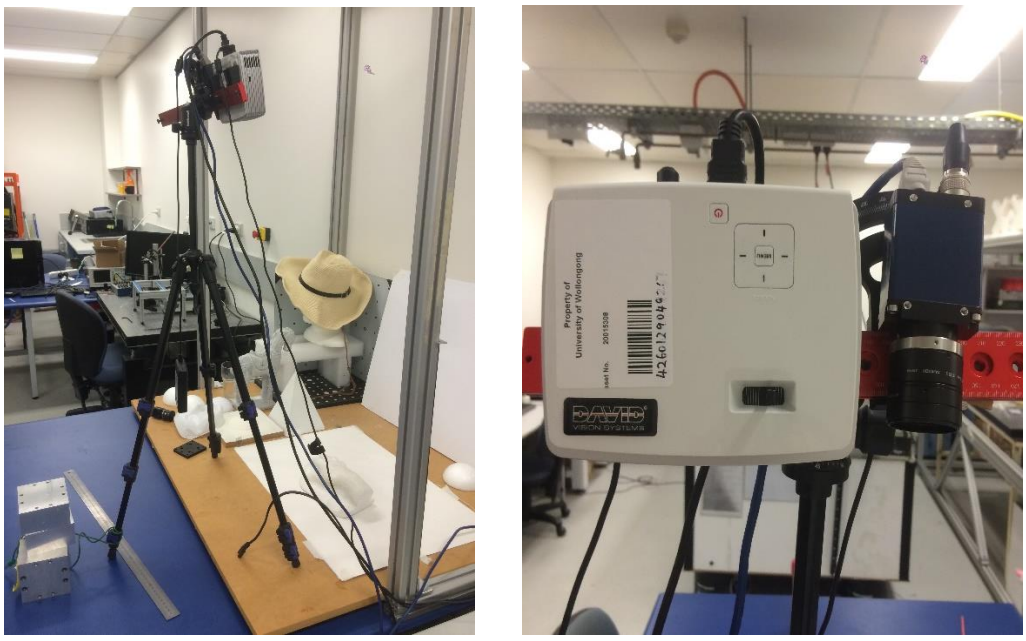

(a) (b)

Fig. 3.1.1 (a) The system for projection fringe profilometry (b) camera and projector.

Aa mentioned above, the FPP method employs a projector and a camera to retrieve the 3D information of the objects with triangle relationship and the

reconstructed results are affected by system establishment and devices parameters, ambient light, selected spatial frequencies, the distances between projector and camera, and others.

In calibration for the system, the camera is calibrated firstly by using the method proposed by Zhang [83]. The camera is described as a pinhole device with internal parameters (focal distance and pixel skew factor), and external parameters (rotation and world coordinate transfer to camera coordinate). The calibration board shown in Fig. 3.1.2 is a board with 9 × 11 circles, and each position are known with high accuracy. During calibration, the camera needs to capture least three positions on the calibration board and the central marks can be extracted. Due to the relative circle marks on the calibration board, it can establish a relationship between camera coordinate system and world coordinate system. Then, the parameters of camera can be obtained.

For projector calibration, the camera is used to capture images from calibration board and compared these images with projector images as if they captured directly by the projector. Then, the projector can be calibrated by the same method used for the camera calibration.

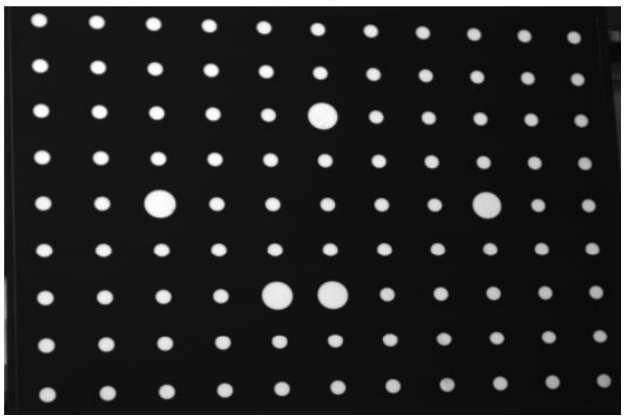

Fig. 3.1.2 calibration board

3.2 Analysis of Simulation and Experiments

To examine the effectiveness of the temporal phase unwrapping method introduced in this chapter, a simulation and some experiments are elucidated and illustrated. The simulation and experiments primarily seek to test whether the Two Selected frequency projection fringe profilometry method are able to reconstruct the value of absolute phase of the object surface.

3.2.1 Simulation of a hemisphere

In the simulation, the phase-shifting of projected patterns are controlled by computer with a fixed value -- $\frac{N}{\pi}$, where N defines the steps of PSP. On that basis, the six-step Phase Shifting Profilometry is used to attain the maps of wrapped phase taking on nonlinear distortion, and a hemisphere is simulated as the object with two selected frequencies which are $f_1 = 5$ and $f_2 = 8$. Firstly, a hemisphere is generated and set in the middle of the reference plane. The size of hemisphere is 300 pixels × 300 pixels. Then, the fringe patterns images for reference plane and object are presented in Fig. 3.2.1.1 (a), (b), (c), and (d). Besides, both the horizontal axis (x-direction) and the vertical axis (y-direction) resolution of pattern image are 1000 in unit pixel(s). Yet no error occurs as the simulation experiment was performed under an ideal situation. To make more practical the simulation results, the impulsive noises are added on the fringe order maps manually by adding or subtracting integer values. In Fig. 3.2.1.1 (e), the selected column y=599 illustrate the fringe order value with impulsive errors when $f_1 = 5$. The distance l_0 is set to 1000mm, and the distance between camera lens and projector lens d_0 is 200mm.

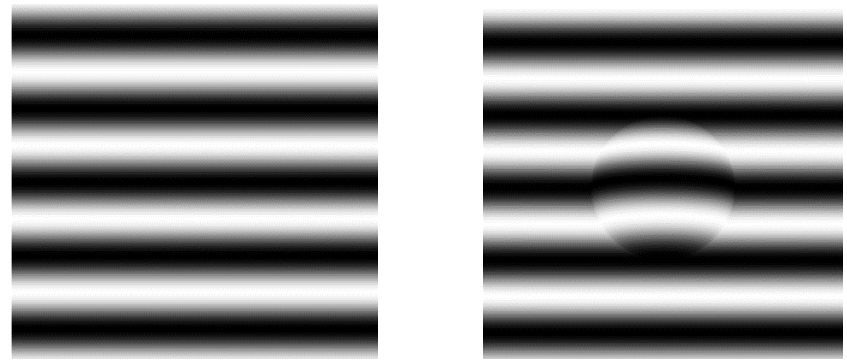

(a)

(b)

(c)

(d)

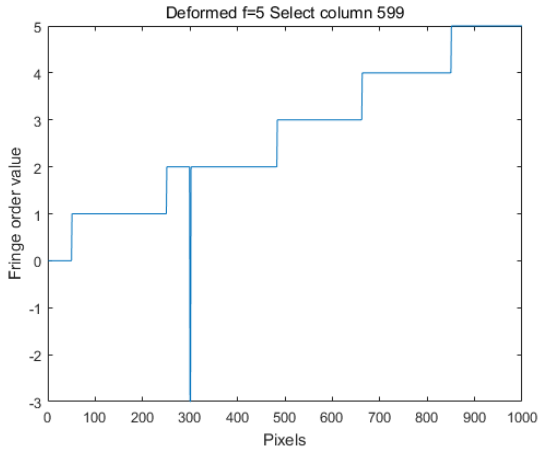

(e)

Fig. 3.2.1.1 Simulation results when $f_1 = 5$ and $f_2 = 8$ (a)-(d) are the reference fringe pattern, deformed pattern for $f_1 = 5$ and $f_2 = 8$ respectively; (e) is the selected column when y=599 for fringe order value with impulsive errors.

Hence, the impulsive errors on fringe order can reflect on wrapped phase maps and absolute phase maps, and then transfer to the 3D reconstruction results.

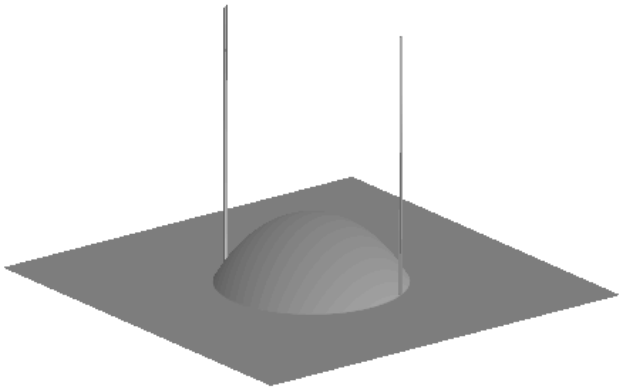

Fig. 3.2.1.2 3D reconstruction results with impulsive errors.

3.2.2 Experiments of a hemisphere

In the experiments, a plastic hemisphere is implemented as the object, and the size of the hemisphere is 95 mm × 95 mm. The measurement system is calibrated before measurement. The vertical (*y*-direction) resolution is 768, and the horizontal (*x*-direction) resolution reaches 1024. The six-step PSP method with two sets of selected frequencies which are $f_1 = 5$ and $f_2 = 8$, $f_1 = 7$ and $f_2 = 13$ in Fig. 3.2.2.1 (a), (b), and (c), (d), respectively.

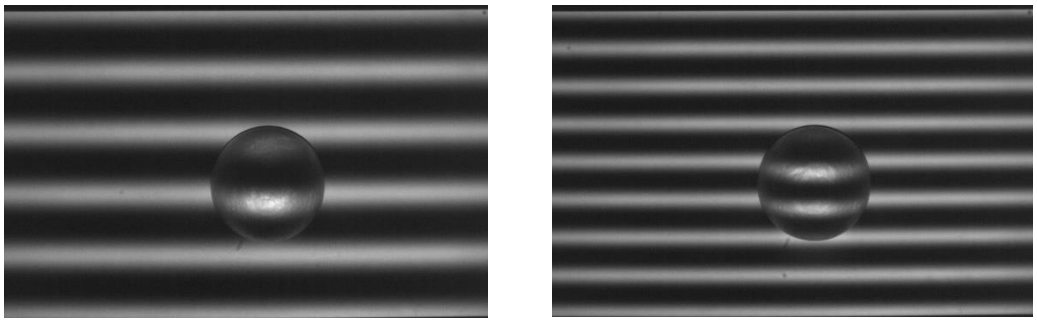

(a) (b)

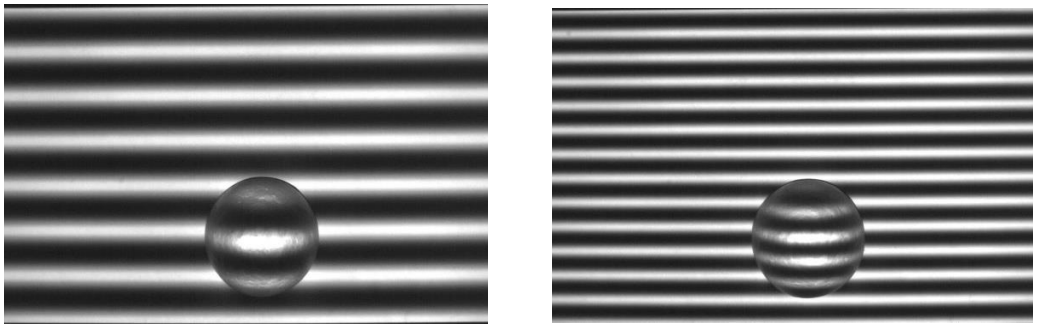

(c) (d)

Fig. 3.2.2.1 Captured patterns for experiments with a plastic hemisphere when (a) $f_1 = 5$, (b) $f_2 = 8$, (c) $f_1 = 7$ and (d) $f_2 = 13$.

The fringe order can be determined using proposed Two Selected frequency projection fringe profilometry for each selected frequency, and presented as below:

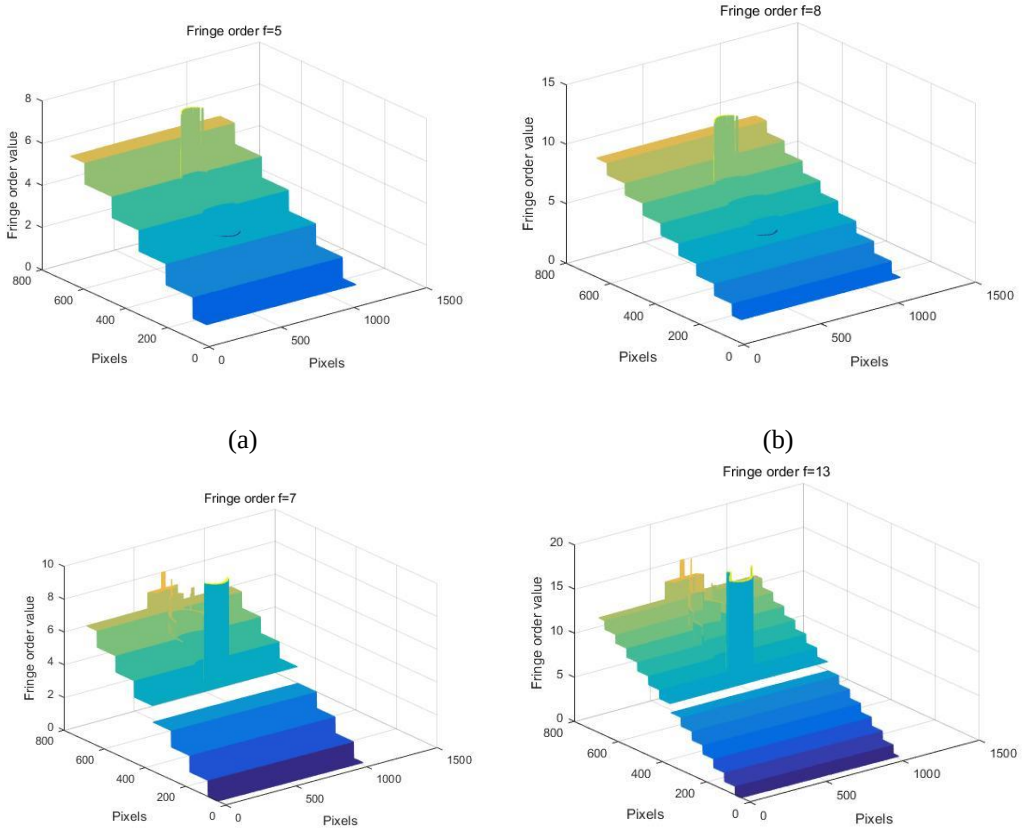

(a) (b)

(c) (d)

Fig. 3.2.2.2 The fringe order values with errors and discontinues (a) $f_1 = 5$, (b) $f_2 = 8$, and (c) $f_1 = 7$,

(d) $f_2 = 13$.

It is acquired from the foregoing figures that the fringe order value can be retrieved through adopting the Two Selected frequency projection fringe profilometry, and the one-one correspondence from $\frac{f_l \phi_h(x,y) - f_h \phi_l(x,y)}{2\pi}$ to fringe order $k_l(x,y)$ and $k_h(x,y)$ can be adopted to reconstruct the absolute phase. Nevertheless, the implosive errors on fringe order shall affect the results on the maps of absolute phase and the 3D reconstruction.

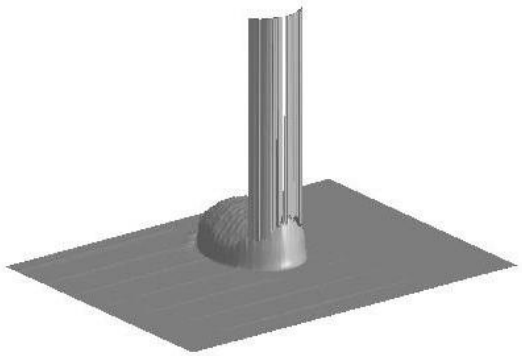

Fig. 3.2.2.3 the 3D reconstruction result with impulsive errors

3.2.3 Experiments of a mask

Comparing with the consecutive surface of the plastic hemisphere, a mask with discontinued or separated surface is employed with 6-step PSP and the size of the mask is approximate 250 mm × 250 mm. In order to achieve high accuracy results for the 3D reconstruction, the measurement system requires the camera to be vertical with the object and reference plane. Then, the system should be calibrated before measurement. The vertical (*y*-direction) resolution is 768, and the horizontal (*x*-direction) resolution reaches 1024. The projected patterns for two sets of selected

frequencies have been presented as following when $f_1 = 5, f_2 = 8$ *and* $f_1 = 7, f_2 = 13$:

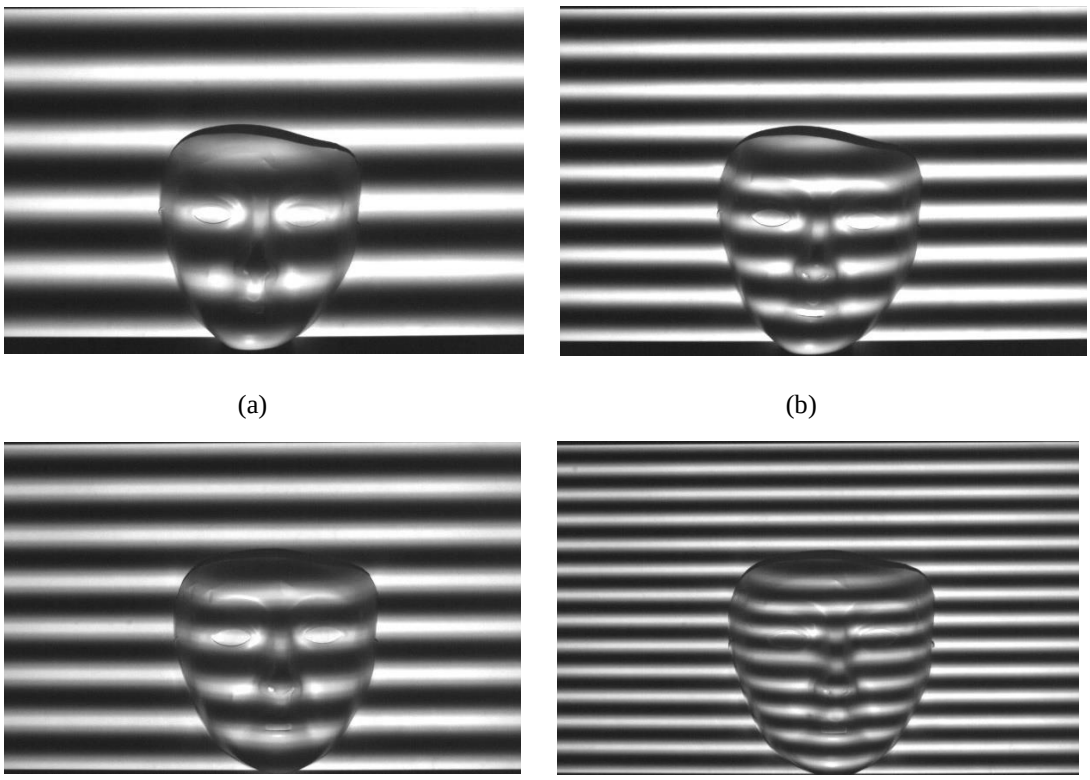

(a) (b)

(c) (d)

Fig. 3.2.3.1 Projected patterns for two sets of selected frequencies for mask when (a) $f_1 = 5$*, (b)* $f_2 = 8$ *and (c)* $f_1 = 7$*, (d)* $f_2 = 13$

The fringe order and absolute phase map can be recovered by the pattern analysis method using the Two Selected frequency projection fringe profilometry, and results are illustrated in Fig. 3.2.3.2. (a)-(h).

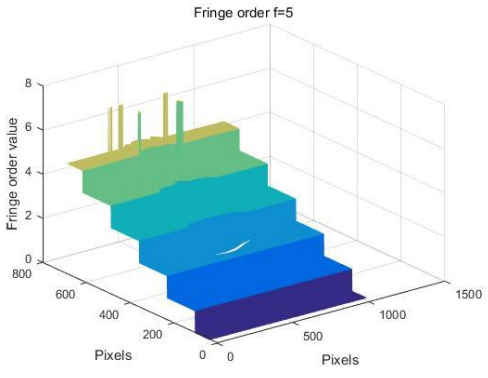

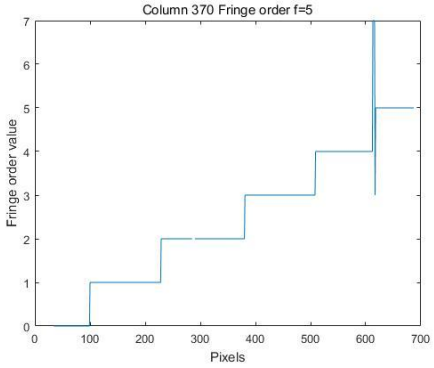

(a) (b)

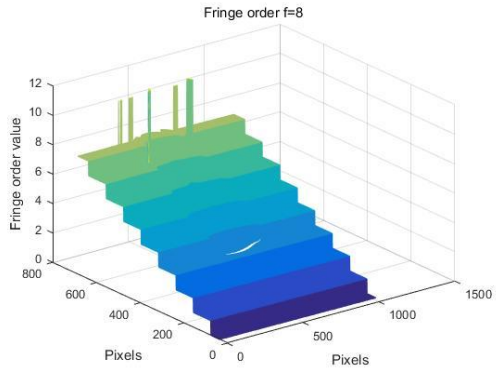

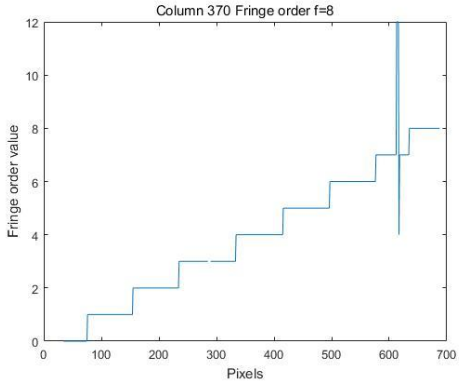

(c) (d)

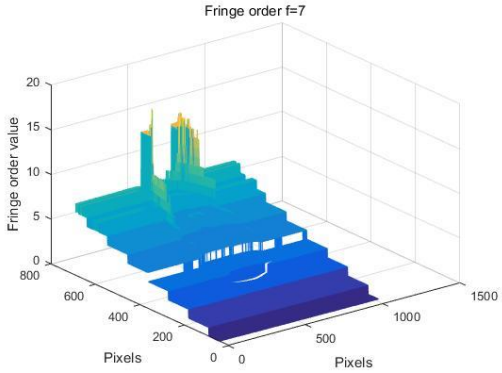

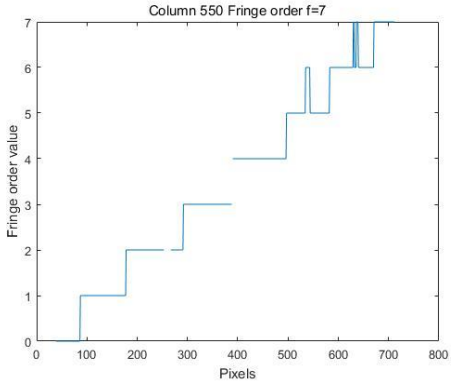

(e) (f)

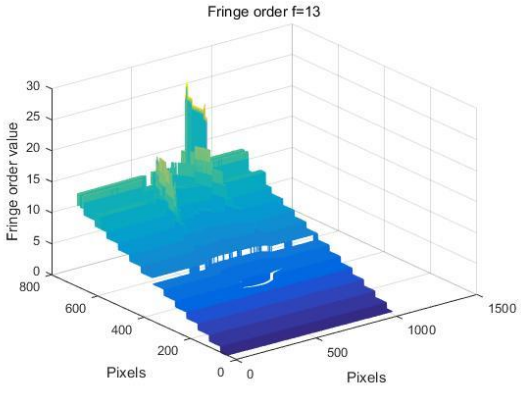

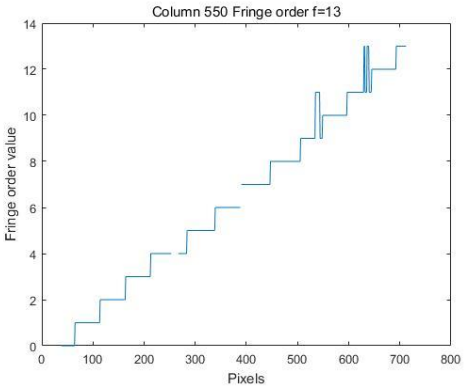

(g) (h)

Fig. 3.2.3.2 Fringe order maps and selected columns (a) $f_1 = 5$; (b) selected column 370 when $f_1 = 5$; (c) $f_2 = 8$; (d) selected column 370 when $f_2 = 8$; (e) $f_1 = 7$; (f) selected column 550 when $f_1 = 7$; (g) $f_2 = 13$; (d) selected column 550 when $f_2 = 13$

It is observed from these results that, the impulsive errors on fringe order for each spatial frequency can be revealed in the absolute phase maps. In this regard, these consecutive impulsive errors can also be reflected at object surface which shown in Fig. 3.2.3.3.

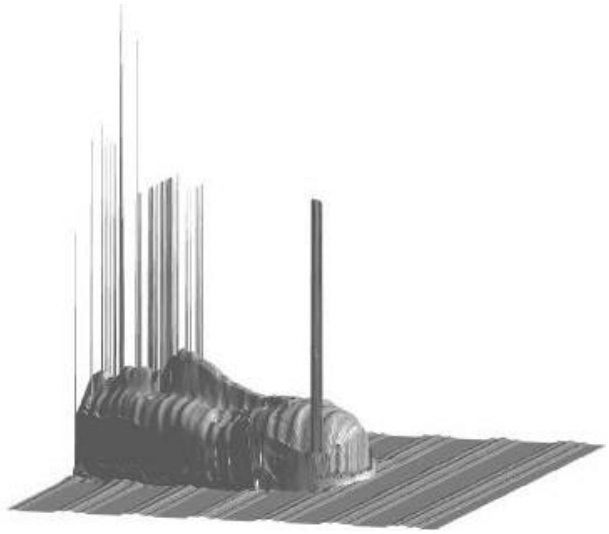

Fig. 3.2.3.3 3D reconstruction result with impulsive errors

3.2.4 Experiment of a horse

In this experiment, the object is a plaster horse which contains lots of separations. These separations generate shadows when the fringe patterns were projected on the object surface, and the proposed Two Selected frequency projection fringe profilometry can retrieve the 3D shape.

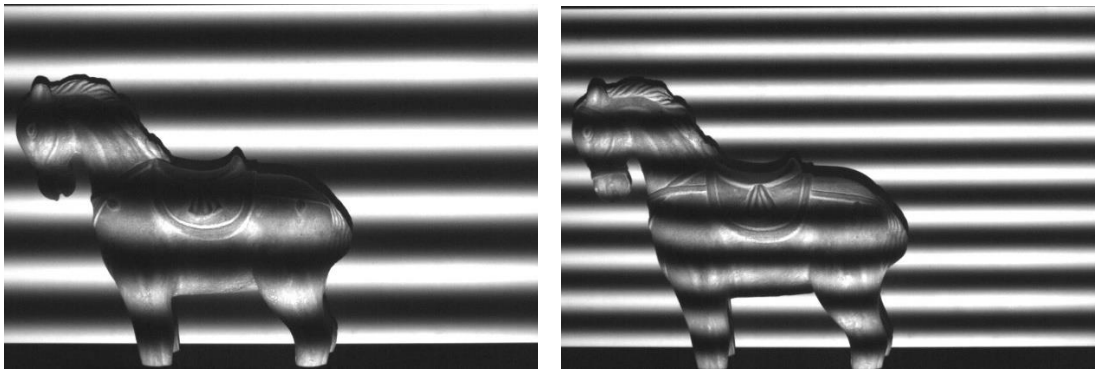

(a) (b)

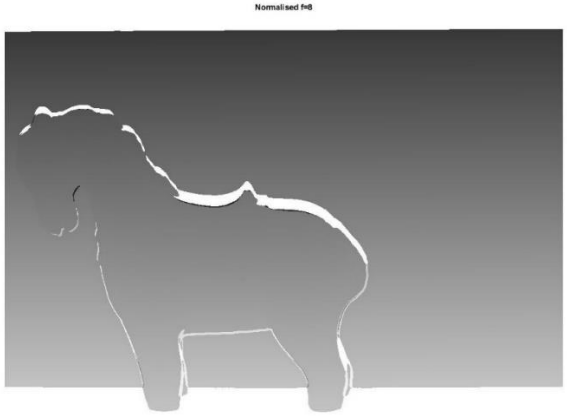

(c)

Fig. 3.2.4.1 Experiment results for horse when (a) $f_1 = 5$, (b) $f_2 = 8$; (c) normalised when $f = 1$

In general, the shadow zones in captured pictures are marked as invalid and shall not be operated which shown as the unnormalised areas in Fig. 3.2.4.1 (c). It is clearly to find that the white area does not contain any height information because of the shadows, and these shadows will transfer to the fringe order maps in Fig. 3.2.4.2 (a) and (b), and 3D reconstruction shown as Fig. 3.2.4.2 (c). The error caused by shadows will not discuss in this thesis.

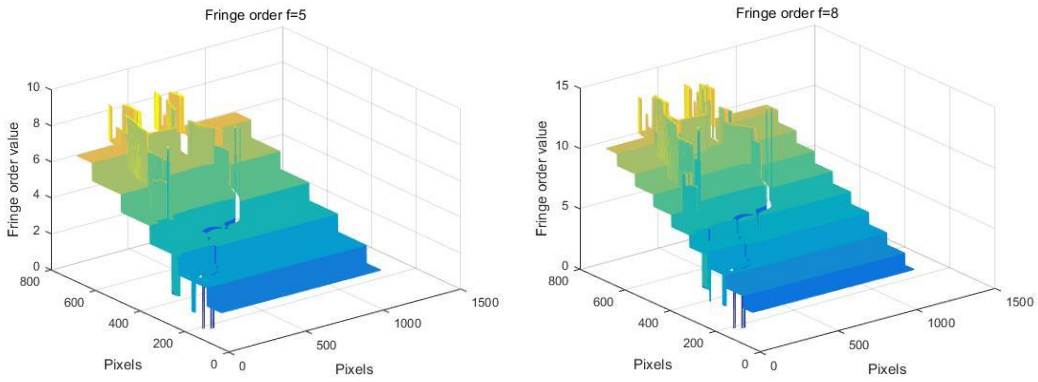

(a) (b)

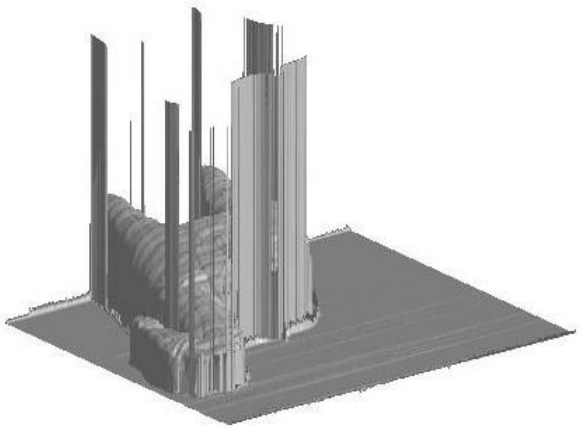

(c)

Fig. 3.2.4.2 The fringe order values with errors for plastic horse when (a) $f_1 = 5$, (b) $f_2 = 8$; (c) 3D reconstruction result with impulsive errors

Hence, from above experiment results, the Two Selected frequency projection fringe profilometry can retrieve the object surface accurately, while some discontinues, and separations still contains many impulsive errors. In this regard, a novel method shall be presented and probed in the next chapter to eliminate the impulsive errors on fringe order specifically.

3.3 Conclusion

This chapter concentrates on the experimental studies for the Two Selected frequency projection fringe profilometry. The experiment set-up is introduced at the beginning. Then, a simulation and experiments are performed to verify the theoretical multi-frequency projection fringe method. From the experiment results, it is clear to see that the fringe order sequence should exhibit a step-wise increase with respect to the direction vertical to the fringes (i.e., x-axis) and step height should always be 1. However, when the surface contains discontinuities or separations, the fringe order sequence will be corrupted by impulsive errors. These errors will affect the results of

3D reconstruction. On the basis of the foregoing operations, a new method shall be provided to analyse and correct the FOE for FPP.

CHAPTER 4: FRINGE ORDER ERROR ANALYSIS AND CORRECTION

4.1 Introduction

The multi-frequency algorithm shall effectively increase the performance taken on by phase unwrapping, whereas phase errors remain, when the wrapped phase maps are corrupted by evident noise or the object surfaces contains steps or discontinues or separations. A framework was proposed by Huntley and Sadner [46] for temporal phase unwrapping, which presents sets of $\log_2 f + 1$based fringe patterns to unwrap a normalised spatial frequency phase map of *f.* A method was proposed by Zhao, *et al.* [38], adopting two sets of fringe patterns, with normal spatial frequency as the one and low spatial frequency pattern as the other taking on absolute phase value in the range $(-\pi, \pi)$. The fringe order can be calculated whereby fringe pattern with low frequency as a reference and map the unwrapped phase. Li, *et al.* [22] used one shot capture image to accelerate the 3D reconstruction, while the gap between two spatial frequencies is evidently bounded, triggering the FOEs. Liu, et al. [63], presents a similar result. A novel method is proposed by Ding, *et al.* [77, 78] to unwrap the temporal phase through using Two Selected frequency fringe patterns to increase the phase error bound effectively. Nonetheless, the bound can be surpassed readily by phase noise in some conditions, triggering impulsive errors in fringe order recovering. Accordingly, a three-fringe pattern with selected spatial frequencies [85] is proposed by Ding, *et al.,* which evidently increases the capability of phase error bound, and recover the fringe order to the greatest extent. Nevertheless, superabundant time is required by different three-fringe patterns to capture for this method, and these patterns are not suitable for real-time 3D reconstruction.

The fringe order for 3D phase retrieval in temporal phase unwrapping is ideal to develop and increase accuracy. Huang, et al [86], presents an identification framework for phase unwrapping and phase error using the phase shifting and compared the phase relationship between neighbouring pixels. Yet the FOE could not be found accurately due to the large absolute phase range criterion in [61]. Zhang, *et al.* [87] proposed a multi-frequency fringe projection method to correct the FOE for a dual-frequency phase unwrapping algorithm. The highest quality pixel is selected as original pixel. In addition, corresponding fringe order is deemed correct. On that basis, a threshold value of original pixel and adjacent pixels shall be established to analyse with the differences. The adjacent pixel considered as a new original pixel when difference is less than threshold value and the fringe order is considered as correct, while the fringe order shall be defined as wrong. Yet this method is time consuming resulting from each pixel in an image need to be compared and evaluated, and hence not suitable for fast 3D profile dynamic measurement.

Based on the foregoing literatures, the FOE has been analysed from existing works, and the key for accurate phase unwrapping is to obtain correct fringe order for each pixel in the phase map. However, the errors can not be completely corrected. Hence, the error correction for fringe order value is extremely important.

This thesis proposed a novel method to improve the accuracy for retrieving the fringe orders. The following sub-chapters shall present this method to correct the errors for the temporal phase unwrapping used for FPP. A medium filter with parameters selected properly is presented to remove the impulsive errors based on stepwise increasing property of fringe order and the impulsive property taken on by

FOEs. Afterwards, a framework to select Sliding Window Size for medium filter and experiments results shall be shown.

4.2 Error Correction Using Median Filter

To correct the FOEs, a sequence $k(x, y)$ shall be factored in. Assume that the fringes parallel to y axis, and $k(x, y)$ shall be progressively increased in line with x, and $k(x, y)$ increases by 1 on the boundary of the two adjacent fringes. When FOEs occur, impulsive errors shall be observed on the $k(x, y)$. In this regard, a median filter can be used to eliminate these errors.

Median filtering is deemed as a signal processing algorithm to effectively eliminate the impulsive noise [88]. As the response to a unit impulse is zero, and the response to step unit remains a step, the median filter takes on superior property to eliminate the impulsive noise and to protect the signal edge. Hence, median filter is very appropriate for eliminating the FOEs, based on the property of ranking pixels contained in the fringe order sequence and replaced by the centre pixel. For these reasons, the following steps are proposed to combat the FOEs:

Step 1: With the phase unwrapped, the fringe order sequence $k(x, y)$ is retrieved;

Step 2: Select the length of the median filter $2N$+1 that shall be evidently smaller than the width of each individual fringe (say 1/10) and prominently outstrip the width of successive fringe errors to find the optimal results. Take a set of $2N$+1 successive samples of (x,) through a sliding window, and apply the median filter to (x,) as follows:

$$K(i) = Med\big(k(i-N), \dots, k(i), \dots, k(i+N)\big), i = N+1, N+2, \dots, M-N \qquad (4.2.1)$$

where $K(i)$ denotes the output of the median filter; $Med()$ refers to the operation to extract the element taking on the median value among the set, and M denotes the total amount of pixels in x-axis.

Step 3: Repeat Step 2 from i=N+1 to $M-N$. It is noteworthy that the above fails to correct the errors in the first and the last N pixels.

The above refers to the standard median filter, which can remove impulsive noises for a large range of signals. Given the step-wise increase of the fringe order sequence, the filter can be modified. Without errors, the sliding window size on fringe order sequence is set which only takes on two possible integer values, that is, the sliding window size is always less than pixels on one fringe order. Accordingly, the following steps are prioritised:

Step 1: Starting from i=N, taking a sliding window of data samples [($i-N$), …, $k(i)$, …, $k(i+N)$], the fringe order for pixel i is identified as K;

Step 2: Moving the sliding window by one pixel, and count the number of K's and the number of K+1's, denoting them by P_k and respectively, the fringe order for pixel i+1 is attained as:

$$K(i+1) = K(i), if\ P_k P_{k+1} > P_{k+1}, otherwise\ K(i+1) = K(i) + 1 \qquad (4.2.2)$$

From the above processes, the proposed method inherits the advantage of PSP and fringe order errors can be eliminated by using median filter. This method enables the accurate correction and can correct the impulsive errors in specified pixels. Due to the stepwise increase property of fringe order and impulsive nature of fringe order errors, the medium filter with properly parameters can completely remove the

impulsive errors. It increases accuracy and efficiency for measurement and reduce the computational cost.

4.3 Selection of Sliding Window Size

With the impulsive errors detection and median filter correction, the FOE can be evident eliminated. Nevertheless, with the different projection conditions, the precise selection of sliding window size for median filter method is very important. To find optimum solution above, we consider a short sequence s(x,y) to denote the pixel number when fringe order $k(x,y)$ is 1, and w(x,y) denotes window size. The short sequence s(x,y) is equal or less than the pixel number for other fringe orders, and the sliding window is established at odd number size which reduce the filtering process and redundant calculation errors. Furthermore, the value of selected window size cannot be excessively small (e.g. w(x,y) equal 3, 5, or 7) as an impulsive error might occur in successive pixels. In this regard, given the foregoing characteristics and the three situations in Chapter 2, different selection of sliding window size can be reckoned with below:

Statement 1: When single pixel FOE appears as a one-pixel pulse in the fringe order map, the sliding window size of median filter is simple and the sliding window can be selected as a minor odd number, e.g. 13 and 15, and w(x,y) should excess 5 pixels and under s(x,y).

Statement 2: When multiple successive pixels occur on fringe order ranging from (t, t+N), the impulsive errors on fringe order shall occur with in excess of one pixel. The window size should be selected as a larger odd number. Basically, the successive pixel errors N is less than the pixel number of

corresponding fringe order's pixels, where w(x,y) is required to surmount 2N-1 and be less than s(x,y).

Statement 3: When the FOEs occur on the boundary of adjacent fringes, the sliding window size is required to be selected in line with different situations. The errors on stepwise increase boundary can be completely recovered by the characteristic taken on by nonlinear signal processing for median filter (precondition: $7 \leq w(x,y) \leq s(x,y)$).

Statement 4: When the foregoing situations occur simultaneously, the selection of window size should be followed by statement 2.

4.4 Experiments

To prove the performance of the proposed approach, relevant experiments are carried out in this Chapter, inclusive of a simulation on a hemisphere and experiments on a pure white hemisphere, mask, and horse. This thesis aims to illustrate that the proposed median filter technique is capable of eliminating the impulsive error through adopting selected frequencies under ideal conditions. As the second part of experiments indicates, the proposed approach is capable of completely and automatically recovering the impulsive error and optimising the reliability and accuracy for two-selected approaches of spatial frequencies.

The test to be performed in the first experiment refers to a virtual hemisphere with smooth surface, aiming to prove the performance of ideal, continuities, and simple surface object. The second tested objects are selected with surface steps or discontinues or separations. The similarly characterised objects can be found in numerous industrial applications. For this reason, these experiments are adopted to demonstrate universality and effectiveness of the proposed technique.

4.4.1 Simulation Results

In the simulation, a pure and smooth surface hemisphere has been generated in Chapter 3.2.1, and two fringe patterns taking on the selected frequencies $f_1 = 5$ and $f_2 = 8$ are projected onto the reference plane and object surface. In ideal cases of free noise and continuous surfaces, the process is simple and straightforward without FOEs. In this regard, some consecutive impulsive noises are introduced in simulation, and the proposed method of Median filter is adopted to reconstruct 3D shape of object. The selection of sliding window size is in the light of Statement 1 in the frameworks, which is 15. The Fig. 4.4.1.1 (a) and (b) illustrates the fringe order value map with or not with impulsive errors in column 599. The Fig. 4.4.1.1 (c) and (d) shows the simulation results before and after using median filter.

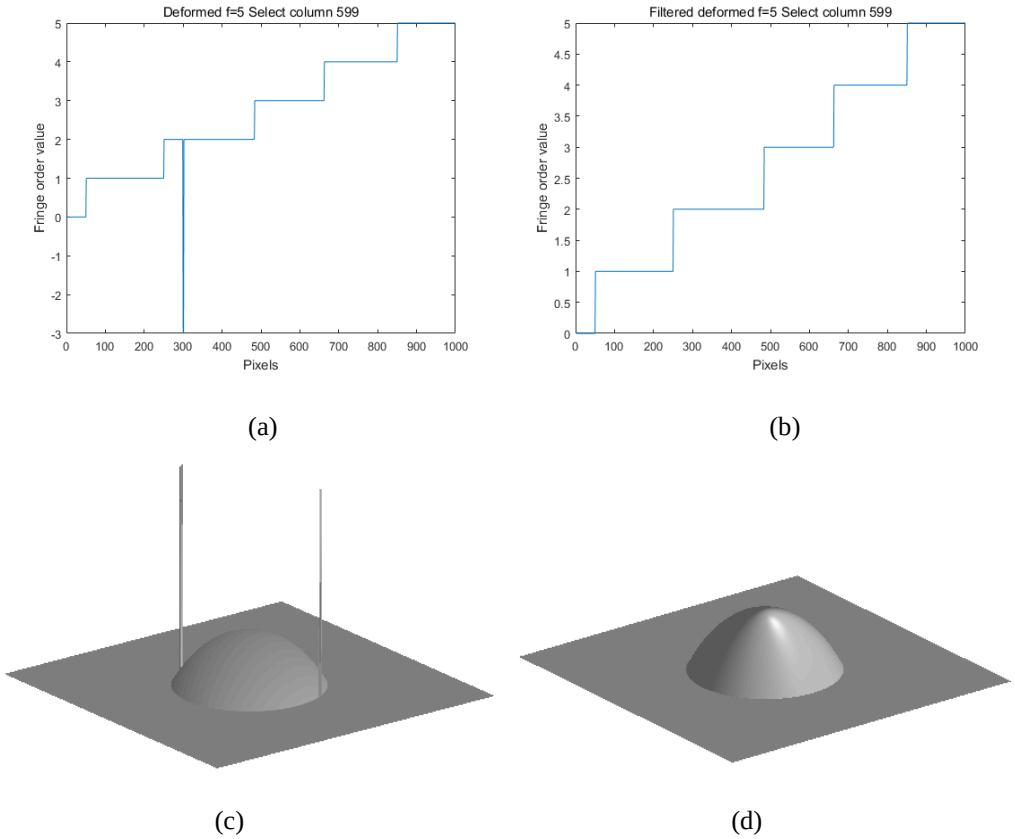

(a) (b)

(c) (d)

Fig. 4.4.1.1 Simulation results when $f_1 = 5$ and $f_2 = 8$ (a) fringe order value with impulsive errors when $f_1 = 5$; (b) fringe order value after median filtering; (c) 3D reconstruction with errors; (d) 3D reconstruction after using median filter.

Hence, the results clearly proved that the impulsive noises can be corrected effectively on fringe order map and there is no error on 3D reconstruction. Yet the simulation only provides an ideal situation which without ambient intensity, γ distortion for captured images, discontinues or separation surface, or another complicated situation. The following experiments shall analyse the actual situation.

4.4.2 Experiment results of a hemisphere

According to the foregoing experiments in Chapter 3.2.2, the first part of this experiment employees a white hemisphere with continuing surface as the object with two selected frequencies $f_1 = 5$ and $f_2 = 8$ onto the reference plane and object surface. Using Two Selected frequency projection fringe profilometry with 6-step PSP and proposed medium filter, the fringe order with impulsive errors can be corrected with window size 15 in Fig 4.4.2.1 (a) and (b). The Fringe order value with selected column y=550 has been shown in Fig. 4.4.2.1 (c) and (d):

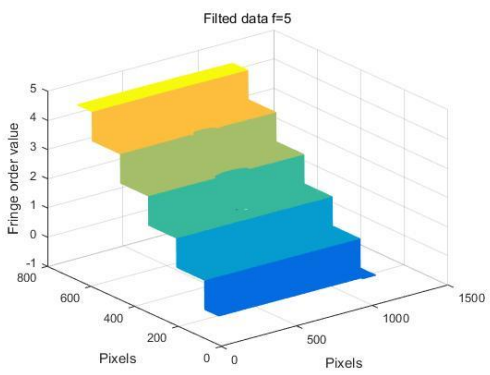

(a)

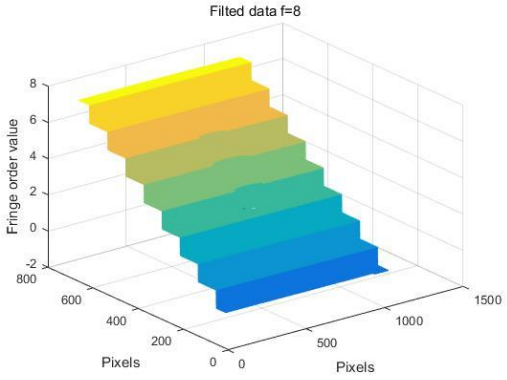

(b)

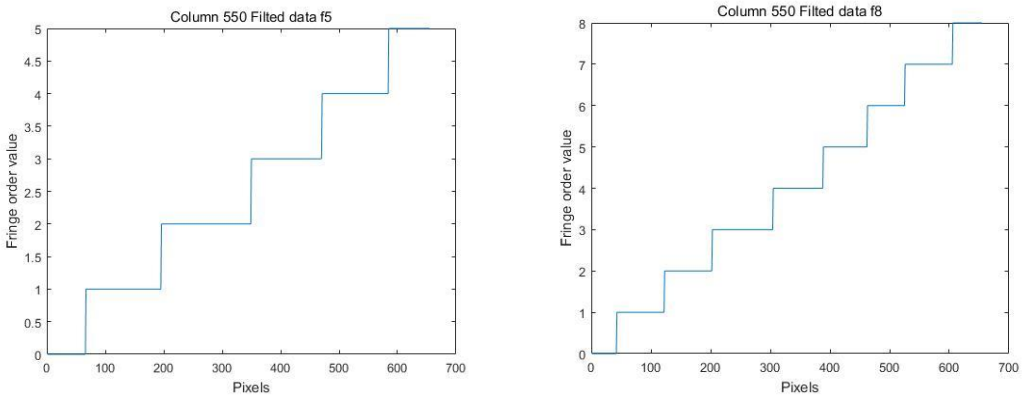

(c) (d)

Fig. 4.4.2.1. Fringe order value after filtering (a) $f_1 = 5$ with error correction; (b) $f_2 = 8$ with error correction; (c) and (d) Fringe order value when with selection y=550

From the above figures, the median filter can eliminate the impulsive errors effectively, and the 3D reconstruction shown in Fig 4.4.2.2 will not carry any impulsive errors.

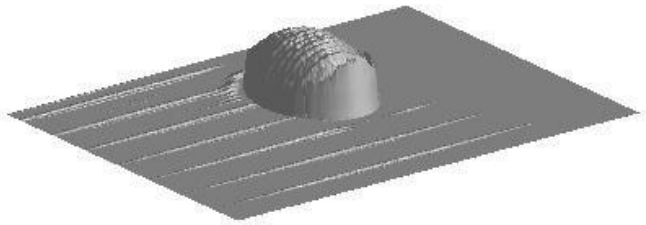

Fig. 4.4.2.2. 3D reconstruction after using Median filter method

The second part, a different set of selected frequencies $f_1 = 7$ and $f_2 = 13$ is used to compare and verified the proposed method. The following Fig. 4.4.2.3 (a) to (c) illustrates the experiment results after median filtering.

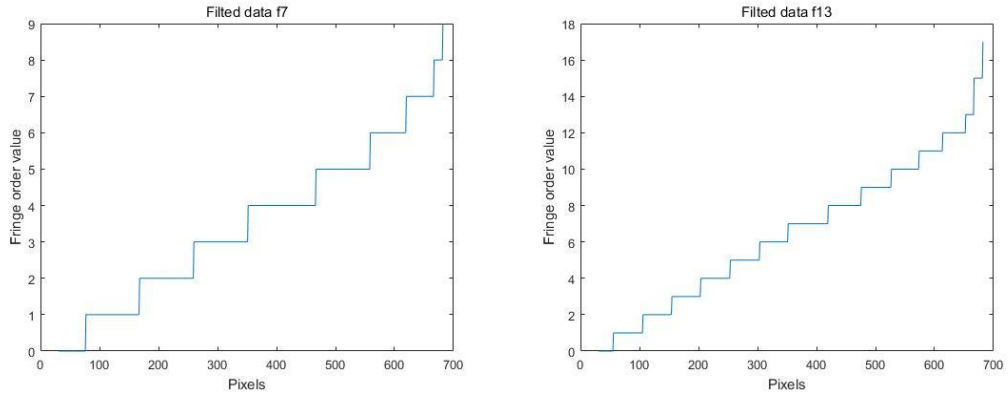

(a) (b)

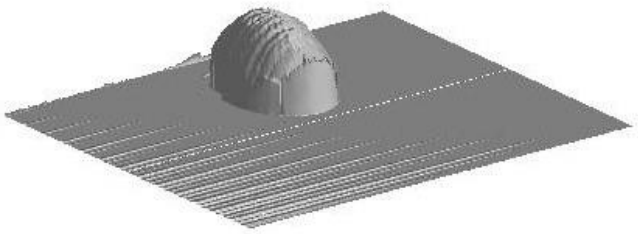

(c)

Fig. 4.4.2.3. Fringe order value after filtering (a) $f_1 = 7$ with error correction; (b) $f_2 = 13$ with error correction; (c) 3D reconstruction after using Median filter method

Hence, the median filter is suitable to eliminate the impulsive noise with superior property and retrieve the 3D reconstruction accurately. Furthermore, comparing with the two different sets of selected frequencies, it can be seen that low frequency set ($f_1 = 5$ and $f_2 = 8$) can either achieve the similar result with high frequency set. In the following experiments, this comparison will still be discussed.

4.4.3 Experiment results of a mask

In this experiment, a mask with discontinues and separations on the surface is used as object based on the experiment and the process is the same in Chapter 3.2.3. The filtered data and reconstruction results have been shown as following:

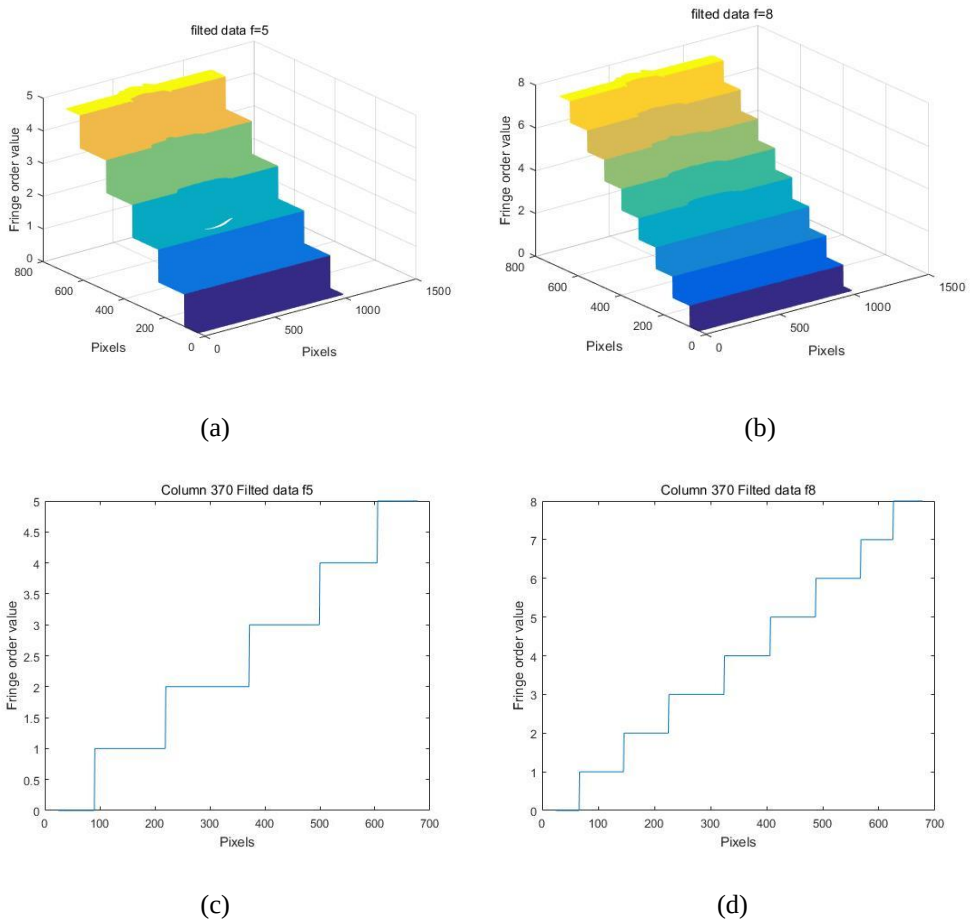

Fig. 4.4.3.1. Fringe order value after filtering (a) $f_1 = 5$ with error correction; (b) $f_2 = 8$ with error correction; (c) and (d) Fringe order value when with selection y=370

The figures 4.4.3.1. (a) and 4.4.3.1. (b) are the fringe order maps after using median filtering with Two Selected frequencies. The figures 4.4.3.1. (c) and 4.4.3.1. (d) are the fringe order values from column 370 for each frequency, respectively. Then, using the proposed algorithm, the mask could be successful reconstructed as following in Fig. 4.4.3.2.

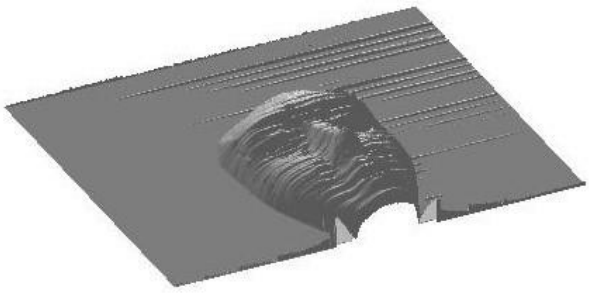

Fig. 4.4.3.2. 3D reconstruction result for mask after using Median filter method

A similar result can be found for another set of selected frequencies when $f_1 = 7$ and $f_2 = 13$ in Fig 4.4.3.3 (a) and (b), which illustrates the experiment after median filtering respectively. It can be seen that the impulsive errors on fringe order have been eliminated, and the sliding window size is selected with 31 based on the Statement 4 in the framework.

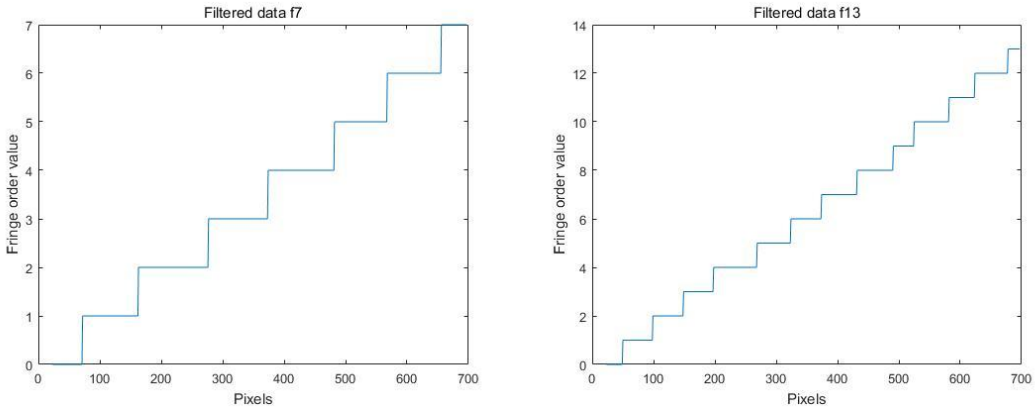

(a) (b)

(c)

Fig. 4.4.3.3. Fringe order value after filtering (a) $f_1 = 7$ with error correction; (b) $f_2 = 13$ with error correction; (c) 3D reconstruction result for mask after using Median filter method

From the figures showing above, the reconstructed results using proposed algorithm can be successfully obtained the shape information with smooth surface reconstruction.

On the basis of the corrected fringe orders whereby median filter, the absolute phase maps and the reconstructed 3D surface of object can be recovered. 3D reconstruction after median filtering method proposed in this thesis is presented in Fig. 4.4.3.3 (c), and no impulsive noise is illustrated on the object surface. It can be found through comparing the experiment results with simulation and hemisphere results that, the actual situation is more complex because the mask model is rougher on surface, and other external influences which lead to more phase unwrapping errors. We can also find that the low frequency set of experiment can save computation cost and achieve effective and accurate results.

4.4.4 Experiment results of a horse

The third experiment employs a white plaster horse which can generate lots of shadows in discontinues and using proposed Median filter method can reduce the impulsive errors in Chapter 3.2.4. In Fig. 4.4.4 (a) and (b), the figures illustrate the fringe order maps with shadows which denote as consecutive values, and the impulsive errors have been eliminated in Fig. 4.4.4 (b) compared with (a).

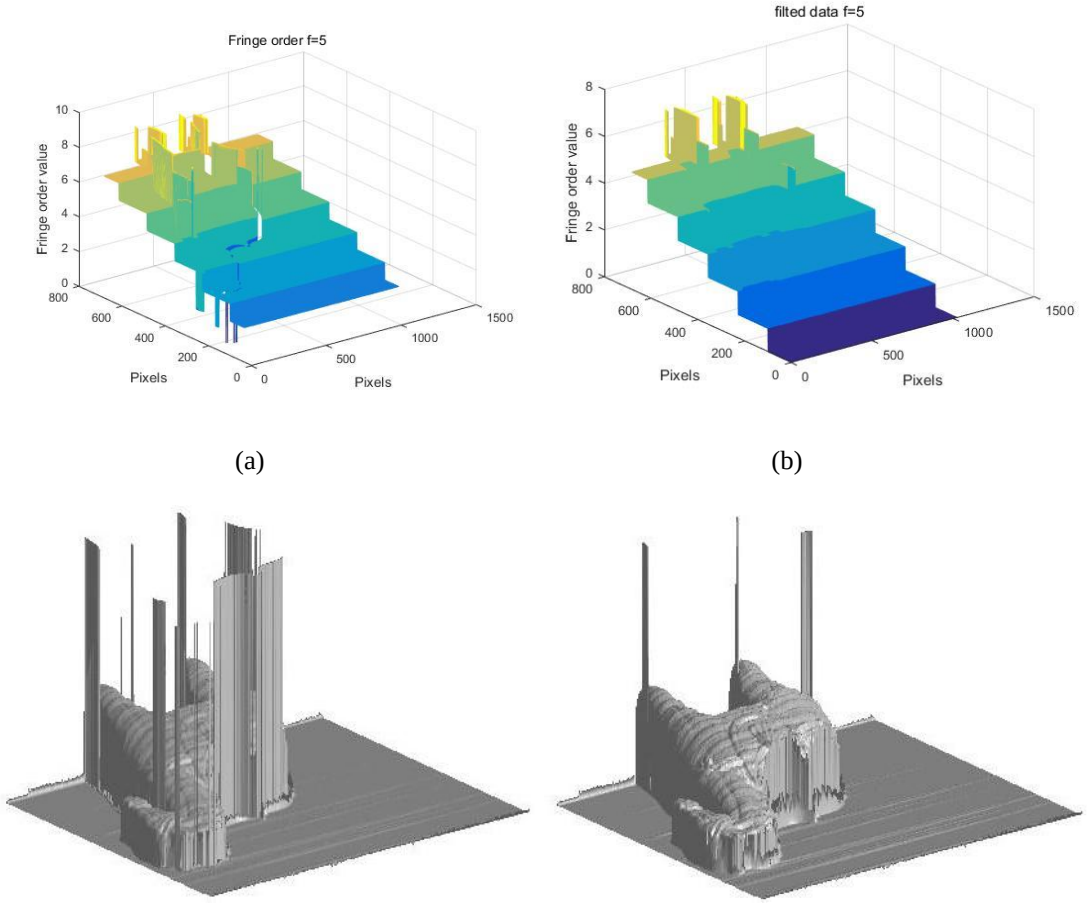

(a) (b)

(c) (d)

Fig. 4.4.4. Comparing fringe order values before and after filtering (a) $f_1 = 5$ with impulsive errors; (b) $f_2 = 5$ with error correction; (c) 3D reconstruction result for horse before using Median filter method; (d) 3D reconstruction after filtering

In Fig. 4.4.4 (c) and (d), the 3D reconstructions have been shown, and the errors have been reduced obviously by using median filtering. It can be seen that the white plaster horse contains the most errors compared with hemisphere and mask because of the complex surface, and this caused by phase unwrapping operation and it will generate more errors.

4.4.5 Experiment results of N-step PSP

Based on above experiments, the Two Selected frequency projection fringe profilometry based on 6-step PSP has been researched and discussed in detail. In this Chapter, the N-step PSP will be studied, especially in 5-step PSP and 4-step PSP. The

white mask is set as the object with selected frequencies $f_1 = 7$ and$f_2 = 13$. The Fig 4.4.5.1 (a) illustrates the 3D reconstruction, and 5-step PSP can either achieve an accurate result compared with 6-step PSP. The Fig 4.4.5.1 (b) can also retrieve the object surface using 4-step PSP, while it can be seen that the Gamma distortion affect the reconstruction result.

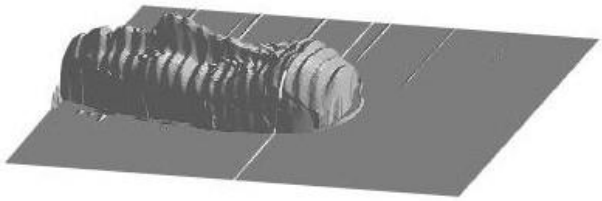

(a)

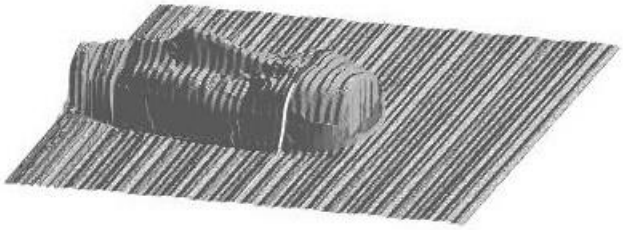

(b)

Fig. 4.4.5 3D reconstruction for (a) 5-step PSP and (b) 4-step PSP

In general, the phase maps obtained by 4-step or 3-stepe PSP method are easier to suffer nonlinear distortion, and this will affect on the $\frac{f_l\phi_h(x,y)-f_h\phi_l(x,y)}{2\pi}$ in rounding calculation. Hence, the correct integer was not fetched with $k_l(x,y)f_h - k_h(x,y)f_l$, and can cause errors. In this regard, if the Gamma distortion can solve the bad influence on phase maps, a 4-step PSP and even 3-step PSP can be used in the future experiments to reduce the calculation cost. In the further application and research, it

can get satisfactory results for FPP according to the specific requirements with appropriate methods.

4.5 Analysis of experiment results

From above experiment results, it can be found that the actual situation is more complex and easier to generate errors than simulation because of impact of ambient light, distortion, and other factors.

For different object surfaces using 6-step PSP, it can be seen that the object with discontinues and separations, such as white mask and plaster horse, contains more errors compared than the hemisphere. The experiment results after correction illustrate that the median filtering can eliminate impulsive errors on fringe order maps effectively and can completely retrieve 3D reconstruction.

For different steps PSP for an object, the 4-step PSP and 3-step PSP can retrieve the 3D shape, respectively after median filtering. However, the Gamma distortion has influenced the reconstruction results. The calculation cost could be reduced if the Gamma distortion can be compensated and reduce the bad influence on phase maps.

4.6 Conclusion

This chapter discussed the proposed median filter method for Two Selected frequency PSP and proposed framework for sliding window size selection in Chapter 4.2 and using some experiments to prove the generality in Chapter 4.4. In accordance with the frequency selection analysis mentioned in Chapter 3, the fringe order and absolute phase map can be retrieved taking on several impulsive errors, and these errors can be reflected on the fringe order and absolute phase map. As the proposed

median filtering is employed with appropriate sliding window, the impulsive errors are eliminated effectively.

To verify the foregoing analysis results, some experiments are performed in this chapter. The simulation seeks to verify that for the general surface continuous objects, the absolute phase can be retrieved in ideal situation whereby simulation. Yet as some impulsive errors are introduced, the median filter can completely eliminate these errors. The experiments seek to prove that the proposed median filtering is suitable and efficient to eliminate the impulsive errors through employing a hemisphere, mask and horse model with large discontinue.

CHAPTER 5: CONCLUSIONS

5.1 Conclusion

This thesis primarily lays the stress on the proposed method of median filter technique for FPP on fringe order impulsive errors correction through using temporal phase unwrapping. Through using our OSPR laboratory**,** extensive work and experiments have been performed to prove the theoretical approach generally.

To expound the problem for impulsive FOEs and correction operation, FPP technique inclusive of approaches to analyse multiple fringe, i.e. FTP and PSP is introduced, spatial phase unwrapping and temporal phase unwrapping in existing phase unwrapping algorithms are compared, and previous works and applications are reviewed. The multi-frequency FPP outstrips single frequency method, and draw upon 3D reconstruction with simple calculation, high speed, and high accuracy. On that basis, the Two Selected Frequency FPP to recover the absolute phase maps by virtue of corresponding relationship between fringe orders is reviewed. Nevertheless, some errors remain, which make the calculation of fringe orders imprecise.

Given the existing problems, a novel method is proposed, serving as a medium filter taking on appropriate parameters to remove the impulsive errors. By virtue of the stepwise increasing property taken on by fringe order and the impulsive property taken on by FOEs, this approach for signal processing is able to effectively eliminate impulsive noise. The framework to select sliding window size for median filter further increases the applicability for multiple impulsive error situations. Subsequently, as the experiment results clearly elucidate, median filter takes on superior property to

remove impulsive noise and protect signal edge, and it increases the reliability of the phase unwrapping result.

5.2 Suggestion for Future Work

This thesis mainly discussed the problems on FPP technique, and a novel method is proposed to correct the impulsive errors associated with fringe orders for the temporal phase unwrapping using Median filter for selected frequencies FPP based on Two Selected frequency method. To satisfy the requirements of more accurate, high speed, real-time 3D reconstruction, it is of critical significance to increase the efficiency of multi-frequency FPP technique. The further research shall lay the following stress particularly:

(1) Gamma distortion and shadow compensation in practical applications

As found when discussing and experimenting in this thesis, the environmental influence, inclusive of ambient light, Gamma distortion of projected fringe patterns, generates shadow stemmed from the special shooting conditions, and the experiments results shall be interference by other external factors. If this thesis seeks to eliminate these external impacts, the results of experiments can be optimised. For instance, phase-error compensation and gamma correction methods can be incorporated for FPP to eliminate errors. Besides, gamma distortion can be reflected on the object surface as illustrated by the results of experiments. Additionally, to compensate the shadow, the fringe patterns with speckle embedded shall be possibly adopted to make regional measurement with multi-frequency fringe patterns, or colour fringe patterns are adopted to compensate shadow areas due to the multi-colour properties.

If the foregoing analysis and test results conform to what it is assumed, this approach can be adopted to increase the efficiency of multi-frequency projection profilometry and to lay a theoretical basis for the practical applications.

(2) How to eliminate strong ambient light and other external factors for FPP

The projected fringe patterns for FPP count as the most critical characteristic ensuring the final experiment results to be accurate. In a strong ambient light environment, e.g. outdoor work, the captured images fail to be high in quality arising from the low signal-to-noise ratio.

REFERENCE

[1] E. Lilienblum, and A. Al-Hamadi, "A structured light approach for 3d surface reconstruction with a stereo line-scan system," *IEEE International Instrumentation and Measurement Technology Conference (I2MTC) Proceedings*, pp. 1171-1176, 2014.

[2] D. Vlasic, P. Peers, I. Baran, P. Debevec, J. Popovic, S. Rusinkiewicz, and W. Matusik, "Dynamic shape capture using multi-view photometric stereo," *in ACM SIGGRAPH Asia*, pp. 1-11, 2009.

[3] Z. Li, B. Curless, and S. M. Seitz, "Spacetime stereo: shape recovery for dynamic scenes," *IEEE Computer Society Conference on Computer Vision and Pattern Recognition*, pp. II-367-74 vol.2, 2003.

[4] J. S. Massa, G. S. Buller, A. C. Walker, S. Cova, M. Umasuthan, and A. M. Wallace, "Time-of-flight optical ranging system based on time-correlated single-photon counting," *Applied Optic*s, vol. 37, no. 31, pp. 7298-7304, 1998.

[5] D. Amad ud, I. A. Halin, and S. B. Shafie, "A review on solid state time of flight TOF range image sensors," *IEEE Student Conference on Research and Development (SCOReD)*, pp. 246-249, 2009.

[6] J. Geng, "Structured-light 3D surface imaging: a tutorial," *Advances in Optics and Photonics*, vol. 3, no. 2, pp. 128-160, 2011.

[7] Q. Xue, Z. Wang, J. Huang, and J. Gao, "Improving the measuring accuracy of structured light measurement system," *Optical Engineering*, vol. 53, no. 11, pp. 112204-112204, 2014.

[8] M.Z. Brown, D. Burschka, and G.D. Hager, "Advances in computational stereo", *IEEE Transactions on Pattern Analysis and Machine Intelligence*, vol. 25, no. 8, pp. 993-1008, 2003.

[9] H. Kawasaki, R. Furukawa, R. Sagawa, and Y. Yagi, "Dynamic scene shape reconstruction using a single structured light pattern," IEEE Conference on Computer Vision and Pattern Recognition, pp. 1-8, 2008

[10] Z. Zhang, D. Zhang, and X. Peng, "Performance analysis of a 3D full-field sensor based on fringe projection," *Optics and Lasers in Engineering*, vol. 42, no. 3, pp. 341-353, 2004.

[11] S. Lei, and S. Zhang, "Flexible 3-D shape measurement using projector defocusing," *Optics Letters*, vol. 34, no. 20, pp. 3080-3082, 2009.

[12] P. Jia, J. Kofman, and C. English, "Two-step triangular-pattern phase-shifting method for three-dimensional objectshape measurement," *Optical Engineering*, vol. 46, no. 8, pp. 083201, 2007.

[13] P. S. Huang, S. Zhang, and F. P. Chiang, "Trapezoidal phase-shifting method for three-dimensional shape measurement," *Optical Engineering*, vol. 44, no. 12, pp. 123601, 2005.

[14] L. Chen, C. Quan, C. J. Tay, and Y. Fu, "Shape measurement using one frame projected sawtooth fringe pattern," *Optics Communications*, vol. 246, no. 4–6, pp. 275-284, 2005.

[15] D. M. Meadows, W. O. Johnson, and J. B. Allen, "Generation of surface contours by moire pattern", *Applied Optics*, vol. 9, no. 4, pp. 942–947, 1970.

[16] X. Su, L. Su, W. Li, and L. Xiang., "New 3D profilometry based on modulation measurement", *Proceedings of SPIE*, vol. 3853, pp. 1–7, 1998.

[17] L. Su, X. Su, W. Li and L. Xiang., "Application of modulation measurement profilometry to objects with surface holes", *Applied Optics*, vol. 38, no.7, pp. 1153-1158, 1999.

[18] C. Wurst, and D. W. Capson., "Surface profile measurement using colour fringe projection", *Machine Vision and Applications*, vol. 4, no. 3, pp.193-203, 1991.

[19] P. Huang, Q. Ho, F. Jin, and F. Chiang., "Colour-enhanced digital fringe projection technique for high-speed 3-D surface countouring", *Optical Engineering*, vol. 38, pp. 1065-1071, 1999.

[20] X. Cheng, X. Su, and L. Guo., "Automated measurement method for 360° profilometry of 3-D diffuse objects", *Applied Optics*, vol. 30, no.10, pp. 1274-1278, 1991.

[21] X. Su, G. von Bally, and D. Vukicevic., "Automated phase-measuring profilometry using defocused projection of a Ronchi grating", *Optics Communications*, vol. 94, no. 6, pp. 561–573, 1992.

[22] M. Takeda, H. Ina, and S. Kobayashi., "Fourier-transform method of fringe-pattern analysis for computer-based topography and interferometry", *Journal of the Optical Society of America A*, vol.72, no.1, pp.156-160, 1982.

[23] M. Takeda and K. Mutoh., "Fourier transform profilomrtry for the automatic measurement of 3-D object shapes", *Applied Optics*, vol. 22, no. 4, pp. 3977-3982, 1983.

[24] P. S. Huang, C. Zhang, and F.-P. Chiang, "High-speed 3-D shape measurement based on digital fringe projection," *Optical Engineering*, vol. 42, no. 1, pp. 163-168, 2003.

[25] P. S. Huang, Q. Hu, F. Jin, and F.-P. Chiang, "Color-encoded digital fringe projection technique for high-speed three-dimensional surface contouring," *Optical Engineering*, vol. 38, no. 6, pp. 1065-1071, 1999.

[26] W.-H. Su, "Color-encoded fringe projection for 3D shape measurements," *Optics Express*, vol. 15, no. 20, pp. 13167-13181, 2007.

[27] H. J. Chen, J. Zhang, D. J. Lv, and J. Fang, "3-D shape measurement by composite pattern projection and hybrid processing," *Optics Express*, vol. 15, no. 19, pp. 12318-12330, 2007.

[28] V. Srinivasan, H. liu, and M. Haliuoua., "Automated phase-measuring profilometry of 3-D diffuse objects", *Applied Optics*, vol.23, no.18, pp. 3105-3108, 1984.

[29] P. Huang, Q. Hu, and F. Chiang., "Double three-step phase-shifting algorithm", *Applied Optics*, vol.41, no.22, pp. 4503-4509, 2002.

[30] I. Ishii, K. Yamamoto, K. Doi, and T. Tsuji, "High-speed 3D image acquisition using coded structured light projection," IEEE International Conference on Intelligent Robots and Systems, pp. 925-930, 2007.

[31] J. L. Posdamer, and M. D. Altschuler, "Surface measurement by space-encoded projected beam systems," Computer Graphics and Image Processing, vol. 18, no. 1, pp. 1-17, 1982.

[32] J. Salvi, J. Pagès, and J. Batlle, "Pattern codification strategies in structured light systems," Pattern Recognition, vol. 37, no. 4, pp. 827-849, 2004.

[33] J. Pan, P. S. Huang, S. Zhang, and F.-P. Chiang, "Color N-ARY gray code for 3-D shape measurement," 12th International Conference on Experimental Mechanics, 2004.

[34] X. Su, and W. Chen, "Reliability-guided phase unwrapping algorithm: a review", *Optics and Lasers in Engineering*, vol. 42, no. 3, pp. 245-261, 2004.

[35] J. M. Huntley, "Noise-immune phase unwrapping algorithm", *Applied Optics*, vol. 28, no. 16, pp. 3260-3270, 1989.

[36] S. Zhang, X. Li, and S. Yau, "Multilevel quality-guided phase unwrapping algorithm for real-time three-dimensional shape reconstruction", *Applied Optics*, vol. 46, no. 1, pp. 50-57, 2007.

[37] S. Li, W. Chen, and X. Su, "Reliability-guided phase unwrapping in wavelet-transform profilometry", *Applied Optics*, vol. 47, no. 18, pp. 3369-3377, 2008.

[38] H. Zhao, W. Chen, and Y. Tan, "Phase-unwrapping algorithm for the measurement of three-dimensional object shapes", *Applied Optics.*, vol.33, pp. 4497-4500, 1994.

[39] J. Li, L. G. Hassebrook, and C. Guan, "Optimized two-frequency phase-measuring-profilometry light-sensor temporal-noise sensitivity", *Journal of the Optical Society of America A*, vol. 20, no. 1, pp. 106-115, 2003.

[40] J. M. Huntley, and H. O. Saldner, "Error-reduction methods for shape measurement by temporal phase unwrapping", *Journal of Optical Society of America A*, vol. 14, no. 12, pp. 3188-3196, 1997.

[41] H. J. Chen, J. Zhang, D. J. Lv, and J. Fang, "3-D shape measurement by composite pattern projection and hybrid processing", *Optics Express*, vol. 15, no. 19, pp. 12318-12330, 2007.

[42] X. Su, A. M. Zarubin, and G. von Bally., "Modulation analysis of phase-shifted holographic interferograms", *Optics Communications*, vol. 105, no. 5, 1994.

[43] J. Li, X. Su, and J. Li., "Phase unwrapping algorithm based on reliability and edge-detection", *Optical Engineering*, vol. 36, no. 6, 1997.

[44] X. Su, G. von Bally, and D. Vukicevic., "Phase-stepping grating profilometry: utilization of intensity modulation analysis in complete object evaluation", *Optics Communications*, vol. 98, no. 141, 1993.

[45] S. Fang, L. Meng, L. Wang, P. Yang, and M. Komori., "Quality-guided phase unwrapping algorithm based on realibility evaluation", *Applied Optics*, vol. 50, no. 28, pp. 5446-5452, 2011.

[46] J. M. Huntley, and H. O. Saldner., "Temporal phase-unwrapping algorithm for automated interferogram analysis", *Applied Optics*, vol. 32, no. 17, pp. 3047-3052, 1993.

[47] J. M. Huntley, and H. O. Saldner., "Shape measurement by temporal phase unwrapping: comparison of unwrapping algorithms", *Measurement Science and Technology*, vol. 8, pp. 986-992,1997.

[48] J. Li, H. Su, and X. Su., "Two-frequency grating used in phase-measuring profilometry", *Applied Optics*, vol. 36, no. 1,1997.

[49] Y. Ding, J. Xi, Y. Yu, and J. Chicharo, "Recovering the absolute phase maps of two fringe patterns with selected frequencies" *Optics Letters*, vol.36, 2011.

[50] Y. Ding, J. Xi, Y. Yu, W. Cheng, S. Wang, and J. F. Chicharo, "Frequency selection in absolute phase maps recovery with two frequency projection fringes," *Optics Express*, vol.20, no.12, pp. 13238–13251, 2012.

[51] G. Sansoni, M. Trebeschi and F. Docchio, "State-of-The-Art and Applications of 3D Imaging Sensors in Industry, Cultural Heritage, Medicine, and Criminal Investigation", *Sensors*, vol. *9*, no.1, pp. 568-601, 2009.

[52] http://www.wikiwand.com/en/Structured-light_3D_scanner Structured-light 3D scanner for a car seat

[53] http://www.proderm.de/en/services/methoden/skin-profilometry.html Skin Profilometry

[54] S. D. Morrison**,** "The Importance of Scleral Shape-Scleral mapping technology and current knowledge of scleral shape affect modern lens design", *Contact Lens Spectrum*, vol. 31, pp. 40-44, 2016.

[55] Y. Wang, L. G. Hassebrook, and D. L. Lau, "Data acquisition and processing of 3D fingerprints", *IEEE Transactions on Information Forensics and Security*, vol. 5, no. 4, 2010.

[56] H. Chen and B. Bhanu, "Human Ear Recognition in 3D", *IEEE Transactions on Pattern Analysis and Machine Intelligence*, vol. 29, no. 4, pp. 718-737, 2007.

[57] D. Zhang, G. Lu, W. Li, L. Zhang, and N. Luo, "Palmprint Recognition Using 3-D Information", *IEEE Transactions on Systems, Man, and Cybernetics, Part C: Applications and reviews*, vol. 39, no. 5, pp. 505-519, 2009.

[58] G. Sansoni, F. Docchio, "3-D Optical Measurements in the Field of Cultural heritage: The Case of the Vittoria Alata of Brescia", *IEEE Transactions on Instrumentation and Measurement*, vol. 54, pp. 359–368, 2005.

[59] X. Su, and W. Chen, "Fourier transform profilometry: a review", *Optics and Lasers in Engineering*, vol. 35, no. 5, pp. 263-284, 2001.

[60] J. Li, X. Su, and L. R. Gup., "An improved Fourier transform profilometry for automatic measurement of 3-d object shapes", *Optical Engineering*, vol.29, no.12, pp. 1439-1444, 1990.

[61] J. Tian, X. Peng, and X. Zhao., "A generalized temporal phase unwrapping algorithm for three-dimensional profilometry", *Optics and Lasers in Engineering*, vol.46, pp.336-342, 2008.

[62] Y. Wang, D. L. Lau, and L. G. Hassebrook, “Fit-sphere unwrapping and performance analysis of 3D fingerprints”. *Applied Optics*, vol. 49, no. 4, pp. 592-600, 2010.

[63] K. Liu, Y.Wang, D. L. Lau, Q. Hao, and L. G. Hassebrook, “Dual-frequency pattern scheme for high-speed 3-D shape measurement”, *Optics Express*, vol. 18, pp. 5229-5244, 2010.

[64] H. Lim, W. Xu, and X. Huang., “Two new practical methods for phase unwrapping”, *International geoscience and remote sensing symposium*, 1995.

[65] D.C. Ghiglia and L.A. Romero., “Minimum l_p-norm two-dimensional phase unwrapping”, *Journal of the Optical Society of America A*, vol. 13, pp. 1999–2013, 1996.

[66] T.J. Flynn., “Two-dimensional phase unwrapping with minimum weighted discontinuity”, *Journal of the Optical Society of America A*, vol. 14, pp. 2692-2701, 1997.

[67] R. M. Goldstein, H. A. Zebker and C. L. Werner., “Satellite radar interferometry: two-dimensional phase unwrapping”, *Radio Science*, vol. 23, pp.713–720, 1988.

[68] S. Inokuchi, K. Sato and F. Matsuda, “Range imaging system for 3-D object recognition”, *Proceedings of the International Conference on Pattern Recognition*, pp. 806–808, 1984.

[69] D. Bergmann, “New approach for automatic surface reconstruction with coded light”, *Proceedings of Remote Sensing and Reconstruction for Three-Dimensional Objects and Scenes*, Vol. 2572, SPIE, San Diego, CA, pp. 2–9, 1995.

[70] D. Zheng and F. Da, “Self-correction phase unwrapping method based on Gray-code light”, *Optics and Lasers in Engineering*, vol. 50, no. 8, pp. 1130-1139, 2012.

[71] J.L. Posdamer and M.D. Altschuler, “Surface measurement by space-encoded projected beam systems”, *Comput. Graph. Image Process*. vol. 18, no. 1, pp. 1–17, 1982.

[72] M. Minou, T. Kanade and T. Sakai, “A method of time-coded parallel planes of light for depth measurement”, *Trans. IECE Jpn*, vol. 64, pp. 521–528, 1981.

[73] D. Caspi, N. Kiryati and J. Shamir, “Range imaging with adaptive color structured light”, *Pattern Anal*, vol. 20, no. 5, pp. 470–480, 1998.

[74] K. Sato, “Range imaging based on moving pattern light and spatio-temporal matched filter”, *IEEE International Conference on Image Processing*, vol. 1, pp. 33–36, 1996.

[75] O. Hall-Holt and S. Rusinkiewicz, “Stripe boundary codes for real-time structured-light range scanning of moving objects”, *The Eighth IEEE International Conference on Computer Vision*, pp. 359–366, 2001.

[76] G. Sansoni, S. Lazzari, S. Peli and F. Docchio, “3d imager for dimensional gauging of industrial workpieces: state of the art of the development of a robust and versatile system”, *International Conference on Recent Advances in 3-D Digital Imaging and Modeling*, Ottawa, Ont., Canada, pp. 19–26, 1997.

[77] Y. Ding, J. Xi, Y. Yu, and J. Chicharo, “Recovering the absolute phase maps of two fringe patterns with selected frequencies” *Optics Letters*, vol.36, 2011.

[78] Y. Ding, J. Xi, Y. Yu, W. Cheng, S. Wang, and J. F. Chicharo, “Frequency selection in absolute phase maps recovery with two frequency projection fringes,” *Optics Express*, vol.20, no.12, pp. 13238–13251, 2012.

[79] F. J. Cuevas, M. Servin, O. N. Stavroudis, and R. Rodriguez-Vera, “Multi-layer neural network applied to phase and depth recovery from fringe patterns,” *Optics Communications*, vol. 181, no. 4–6, pp. 239-259, 2000.

[80] F. Pedersini, A. Sarti, and S. Tubaro, “Accurate and simple geometric calibration of multi-camera systems,” *Signal Processing*, vol. 77, no. 3, pp. 309-334, 1999.

[81] Q. Hu, P. S. Huang, Q. Fu, and F.-P. Chiang, “Calibration of a three-dimensional shape measurement system,” *Optical Engineering*, vol. 42, no. 2, pp. 487-493, 2003.

[82] S. Zhang, and P. S. Huang, “Novel method for structured light system calibration,” *Optical Engineering*, vol. 45, no. 8, pp. 083601, 2006.

[83] Z. Zhang, “A flexible new technique for camera calibration,” *IEEE Transactions on Pattern Analysis and Machine Intelligence*, vol. 22, no. 11, pp. 1330-1334, 2000.

[84] K. Liu, Y. Wang, D. L. Lau, Q. Hao, and L. G. Hassebrook, “Dual-frequency pattern scheme for high-speed 3D shape measurement”, *Optics Express*, vol. 18, no. 5, pp. 5229-5244, 2010.

[85] Y. Ding, J. Xi, Y. Yu, and F. Deng, “Absolute phase recovery of three fringe patterns with selected spatial frequencies”, *Optics and Laser in Engineering*, vol. 70, no. 7, pp. 18-25, 2015.
[86] L. Huang, and A. K. Asundi, “Phase invalidity identification framework with the temporal phase unwrapping method”, *Measurement Science and Technology*, vol. 22, no. 3, 2011.
[87] C. Zhang, H. Zhao, and L. Zhang, “Fringe order error in multifrequency fringe projection phase unwrapping: Reason and correction”, *Applied Optics*, vol. 54, no.32, pp.9390-9399, 2015.
[88] T. Huang, G. Yang, and G. Tang, “A fast two-dimensional median filtering algorithm”, *IEEE Transactions on Speech, Signal Processing*, vol. 27, no. 1, pp. 13-18, 1979.

APPENDIX

A work in this thesis has been submitted as academic papers.

Conference paper:

1. Naixin LI, Jiangtao Xi, Yanguang Yu, Qinghua Guo, Jun Tong, Philip Ogunbona, “Simulation study on improving the spatial resolution of absolute phase map recovered by fringe projection profilometry with the images of different resolutions” has been submitted to International Conference on Optical and Photonic Engineering (icOPEN2018).